

**Neural mechanisms in processing of emotion in real and virtual  
faces using functional-near infrared spectroscopy (fNIRS)**

by

Dylan Rapanan

A thesis submitted to the  
School of Graduate and Postdoctoral Studies  
in partial fulfillment of the requirements for the degree of

**Master of Science in Computer Science**

Faculty of Science  
University of Ontario Institute of Technology (Ontario Tech University)  
Oshawa, Ontario, Canada  
August 2025

© Dylan Rapanan 2025

# **THESIS EXAMINATION INFORMATION**

Submitted by: **Dylan Rapanan**

**Master of Science in Computer Science**

Thesis title: Neural mechanisms in processing of emotion in real and virtual faces using functional-near infrared spectroscopy (fNIRS)

An oral defense of this thesis took place on August 6, 2025, in front of the following examining committee:

**Examining Committee:**

|                              |                         |
|------------------------------|-------------------------|
| Chair of Examining Committee | NAME                    |
| Research Supervisor          | Steven Livingstone, PhD |
| Research Co-supervisor       | Bobby Stojanoski, PhD   |
| Examining Committee Member   | Mehran Ebrahimi, PhD    |
| Thesis Examiner              | Ali Neshati, PhD        |

The above committee determined that the thesis is acceptable in form and content and that a satisfactory knowledge of the field covered by the thesis was demonstrated by the candidate during an oral examination. A signed copy of the Certificate of Approval is available from the School of Graduate and Postdoctoral Studies.

# Abstract

As avatars permeate social media, gaming, and telecommunications, understanding how the brain reads emotions from virtual faces is increasingly important. We recorded functional near-infrared spectroscopy (fNIRS) data from adults viewing real photographs and matched computer-generated faces expressing Anger, Disgust, Fear, Joy, Sadness, Surprise, or Neutral (control). General-linear-model mapping revealed higher activation in virtual faces in the left occipital region, and higher activation in Neutral and Surprise compared to the other emotions in parietal and occipital regions. Functional-connectivity analysis revealed higher connectivity in real faces across the brain, and higher connectivity across the brain in Anger and Fear compared to the other emotions. Collectively, the results demonstrate differences in activation in occipital areas, and differential processing of face and emotion types across the whole brain. These neural signatures provide quantitative targets for refining the realism and emotional efficacy of digital characters in virtual and augmented environments.

**Keywords:** Virtual faces; Emotion perception; Functional near-infrared spectroscopy (fNIRS); Functional connectivity; Brain networks

## **Author's Declaration**

I hereby declare that this thesis consists of original work of which I have authored. This is a true copy of the thesis, including any required final revisions, as accepted by my examiners.

I authorize the Ontario Tech University to lend this thesis to other institutions or individuals for the purpose of scholarly research. I further authorize the Ontario Tech University to reproduce this thesis by photocopying or by other means, in total or in part, at the request of other institutions or individuals for the purpose of scholarly research. I understand that my thesis will be made electronically available to the public.

The research work in this thesis that was performed in compliance with the regulations of Research Ethics Board under REB Certificate number 17656.

Dylan Rapanan

## **Statement of Contributions**

I hereby certify that I am the sole author of this thesis and that no part of this thesis has been published or submitted for publication. I have used standard referencing practices to acknowledge ideas, research techniques, or other materials that belong to others. Furthermore, I hereby certify that I am the sole source of the creative works and/or inventive knowledge described in this thesis.

## Acknowledgements

# Contents

|   |     |
|---|-----|
| <b>Thesis Examination Information</b>                       | ii  |
| <b>Abstract</b>   | iii |
| <b>Author's Declaration</b>                                 | iv  |
| <b>Statement of Contributions</b>                           | v   |
| <b>Acknowledgments</b>                                      | vi  |
| <b>Table of Contents</b>                                    | vii |
| <b>List of Tables</b>                                       | ix  |
| <b>List of Figures</b>                                      | x   |
| <b>List of Abbreviations and Symbols</b>                    | xii |
| <b>1 Introduction</b>                                       | 1   |
| 1.1 Facial Emotion Perception . . . . .                     | 2   |
| 1.2 Real vs. Virtual (Avatar) Face Perception . . . . .     | 5   |
| 1.3 Functional Near-Infrared Spectroscopy (fNIRS) . . . . . | 7   |
| 1.4 Objectives and Hypotheses . . . . .                     | 9   |

|   |           |
|---|-----------|
| <b>2 Methodology</b>  | <b>11</b> |
| 2.1 Participants . . . . .  | 11        |
| 2.2 Stimuli and apparatus . . . . .                                   | 13        |
| 2.2.1 Stimuli . . . . .   | 13        |
| 2.2.2 Apparatus . . . . .   | 13        |
| 2.3 Design and procedure . . . . .                                    | 15        |
| 2.3.1 Design . . . . .  | 15        |
| 2.3.2 Procedure . . . . .   | 15        |
| 2.4 Analyses . . . . .  | 16        |
| 2.4.1 fNIRS preprocessing . . . . .                                   | 17        |
| 2.4.2 Activation magnitude with General Linear Model (GLM) . . . . .  | 19        |
| Design Matrix . . . . .   | 19        |
| Contrast Computation . . . . .  | 20        |
| 2.4.3 Network mapping with Functional Connectivity Analysis . . . . . | 21        |
| Paired Sample t-tests . . . . .                                       | 22        |
| ROI Chord Plots . . . . .   | 22        |
| Emotion Summary Ratio Plot . . . . .                                  | 23        |
| Region Summary Plot . . . . .   | 23        |
| 2.4.4 Memory Task Analysis . . . . .                                  | 24        |
| <b>3 Results</b>  | <b>25</b> |
| 3.1 Neural activation magnitude . . . . .                             | 25        |
| 3.2 Functional Connectivity Mapping . . . . .                         | 29        |
| 3.3 Memory Task Results . . . . .                                     | 36        |
| <b>4 Discussion</b>   | <b>38</b> |
| 4.1 Limitations and Future Directions . . . . .                       | 45        |
| 4.2 Conclusion . . . . .  | 46        |

|  |           |
|--|-----------|
| <b>Bibliography</b>                                | <b>46</b> |
| <b>Data Availability</b>                           | <b>58</b> |
| <b>Appendix</b>                                    | <b>58</b> |
| <b>A GLM Contrasts</b>                             | <b>59</b> |
| <b>B Functional Connectivity Contrasts</b>         | <b>64</b> |
| <b>C Memory Task</b>                               | <b>74</b> |
| C.1 ANOVA Results . . . . .                        | 74        |
| C.2 Memory Task No Response Distribution . . . . . | 75        |
| <b>D Ethics Approval Letters</b>                   | <b>76</b> |
| D.1 REB Approval . . . . .                         | 77        |
| D.2 REB Renewal . . . . .                          | 79        |

# List of Tables

|     |   |    |
|-----|---|----|
| A.1 | Table of significant contrast results from the GLM analysis.  | 59 |
| B.1 | Ratio of positive to negative $t$ -values for each contrast. The ratio is calculated as Ratio = (Number of Positive $t$ -values - Number of Negative $t$ -values) / (Number of Positive $t$ -values + Number of Negative $t$ -values).<br>For condition1 - condition2, a positive ratio indicates that condition1 has more positive $t$ -values than condition2, while a negative ratio indicates the opposite. | 67 |
| C.1 | Two-way ANOVA results for the effect of Face Type and Emotion and their interaction on the correct responses.   | 74 |

# List of Figures

|      |   |    |
|------|---|----|
| 2.1  | Participant signal quality and inclusion flow . . . . .             | 12 |
| 2.2  | Montage and brain region map . . . . .                              | 14 |
| 2.3  | Experimental paradigm overview . . . . .                            | 16 |
| 2.4  | Preprocessing steps for fNIRS data . . . . .                        | 17 |
| 2.5  | Sample design matrix for GLM . . . . .                              | 20 |
| 3.1  | GLM: Real vs. Virtual Faces . . . . .                               | 25 |
| 3.2  | GLM: Emotion vs. Neutral . . . . .                                  | 26 |
| 3.3  | GLM: Emotion vs. Surprise . . . . .                                 | 27 |
| 3.4  | GLM: Face Type $\times$ Emotion Contrasts . . . . .                 | 28 |
| 3.5  | FC: Real vs. Virtual . . . . .                                      | 29 |
| 3.6  | FC: Emotion Contrasts . . . . .                                     | 30 |
| 3.7  | FC: Summary of Contrasts by Emotion Pair . . . . .                  | 32 |
| 3.8  | FC: Count of Significantly Different Channel Pairs by ROI . . . . . | 33 |
| 3.9  | FC: Face Type $\times$ Emotion Contrasts . . . . .                  | 35 |
| 3.10 | Correct Memory Task Responses by Face Type and Emotion . . . . .    | 37 |
| B.1  | FC: Additional emotion contrasts . . . . .                          | 64 |
| C.1  | Memory Task No Response Distribution . . . . .                      | 75 |
| D.1  | REB Approval Letter (First Page) . . . . .                          | 77 |
| D.2  | REB Approval Letter (Second Page) . . . . .                         | 78 |

|     |   |    |
|-----|---|----|
| D.3 | REB Renewal Request Approval Letter (First Page) . . . . .  | 79 |
| D.4 | REB Renewal Request Approval Letter (Second Page) . . . . . | 80 |

# List of Abbreviations and Symbols

|       |                                       |
|-------|---------------------------------------|
| AUs   | Action Units                          |
| BOLD  | Blood-Oxygenation-Level-Dependent     |
| CWT   | Continuous Wavelet Transform          |
| DCT   | Discrete Cosine Transform             |
| dlPFC | Dorsolateral Prefrontal Cortex        |
| ERP   | Event-Related Potential               |
| FACS  | Facial Action Coding System           |
| fMRI  | Functional Magnetic Resonance Imaging |
| fnIRS | Functional Near-Infrared Spectroscopy |
| GLM   | General Linear Model                  |
| HbO   | Oxyhemoglobin                         |
| HbR   | Deoxyhemoglobin                       |
| HbT   | Total Hemoglobin                      |
| HRF   | Hemodynamic Response Function         |
| ISI   | Inter-Stimulus Interval               |
| LPP   | Late Positive Potential               |
| MVPA  | Multivariate Pattern Analysis         |
| OLS   | Ordinary Least Squares                |
| PFC   | Prefrontal Cortex                     |
| PSP   | Peak Spectral Power                   |

|         |                                       |
|---------|---------------------------------------|
| RADIATE | Racially Diverse Affective Expression |
| ROI     | Region of Interest                    |
| SCI     | Scalp Coupling Index                  |
| SPM     | Statistical Parametric Mapping        |
| WTC     | Wavelet Transform Coherence           |

# Chapter 1

## Introduction

Our brains appear primed to process faces (Johnson et al., 1991; Palmer and Clifford, 2020; Powell et al., 2018). This privileging of facial information speaks to the face's central role in our social life, conveying information on our identity, intent and affect (Sheehan and Nachman, 2014; Cowen et al., 2021; Willis and Todorov, 2006). Among these signals, emotional expressions are especially consequential, enabling observers to infer the internal states of others and to co-ordinate behaviour in real time. However, despite a rich literature on emotion perception, it remains unclear the brain involved in the processing of emotional expressions (Barrett, 2006a). This lack of clarity is particularly relevant as our interactions shift increasingly toward digital platforms featuring virtual representations of human faces.

There has been a dramatic increase in the use of avatars, computer-generated representations of humans, across a wide range of platforms, including social media, video games, virtual reality (VR), and augmented reality (AR). As interactions with avatars become more prevalent, particularly in applications involving communication and social interaction, their ability to convincingly express human-like emotions has become a subject of growing interest (Kegel et al., 2020). The capacity of avatars to produce recognizable and appropriate facial emotional expressions is key to their social acceptance

and utility.

Unlike real human faces, which convey emotion through a complex interplay of subtle muscle movements, virtual faces must rely on pre-programmed or algorithmically generated expressions. These expressions may differ in perceived realism, dynamicity, and authenticity, potentially altering how they are processed by the brain. This raises several important questions: Does processing virtual facial expressions engage the same neural mechanisms as processing real facial expressions? Do different emotional expressions elicit distinct neural responses in the brain? And finally, is processing emotional expressions in virtual faces fundamentally different from processing emotional expressions in real faces? To address these questions, this thesis investigates the neural mechanisms underlying facial emotion perception in both real and virtual faces using functional near-infrared spectroscopy (fNIRS).

## 1.1 Facial Emotion Perception

Emotion perception involves recognizing social cues such as facial emotional expressions, which is the focus of this thesis. Human facial emotion perception has been a central topic in affective neuroscience, having identified a set of basic emotions that are universally recognized across cultures ([Ekman and Friesen, 1971](#)). Ekman proposed six basic emotions: happiness, sadness, anger, fear, disgust, and surprise, with neutral faces serving as a baseline. These emotions are reliably associated with distinct facial configurations, known as the Facial Action Coding System (FACS), which provides a comprehensive taxonomy of facial muscle movements, known as action units, which underpin the visible expressions of emotion ([Ekman and Friesen, 1978](#)). FACS categorizes facial movements into action units (AUs), each corresponding to specific muscle contractions, such as the raising of the eyebrows or the curling of the lips. Substantial evidence supports the universality and biological roots of these basic emotions. Seminal cross-cultural field studies

conducted by in the late 1960s/70s found that preliterate populations in Papua New Guinea reliably recognized and produced the same six expressions identified in Western populations, despite having had no exposure to media (Matsumoto and Wilson, 2022). These studies used both posed expressions and spontaneous reactions (e.g., watching distressing films), highlighting that these expressions are natural responses rather than learned social habits. While universality is well supported, it is far from the whole story. More recent research using advanced computer graphics and mental reconstruction methods has shown that Eastern and Western observers may mentally represent the intensity and specific facial actions of basic emotions differently, with Eastern observers representing emotional intensity with more distinctive dynamic eye activity (Jack et al., 2012). This leads to the idea of "cultural dialects" in emotional expression, where the core muscular movements are conserved, but cultural nuances in expression and interpretation vary (Ruttkay, 2009). These findings suggest that while the basic emotions and their associated facial expressions are universal, cultural factors influence how these emotions are expressed and perceived.

More recent approaches, however, advocate a constructionist view of emotion. This constructionist view posits that emotions are not fixed categories, but constructed experiences emerging from the brain's interpretation of internal and external stimuli (Barrett, 2006b). It argues that emotions arise from distributed and context-sensitive patterns of neural activity involving domain-general brain networks rather than discrete, emotion-specific regions (Lindquist et al., 2012). Crucially, behavioral studies show that context routinely shapes emotion perception, not only in ambiguous situations but even when expressions appear prototypical. For example, neutral faces are often experienced as fearful, happy, or sad depending on whether they follow scenes of fear or joy, demonstrating that context significantly biases both valence and categorical interpretation of facial expressions (Calbi et al., 2017). Other research shows that emotion labels activate conceptual knowledge, which then guides the integration of facial cues and context before

an emotion category is consciously assigned—even for clear, non-ambiguous expressions (Brooks and Freeman, 2018). This influence of context is automatic and difficult to suppress, even when participants are explicitly told to ignore contextual cues, or while performing a secondary cognitive task, context continues to shape how they perceive facial emotions (Aviezer et al., 2011). Moreover, cultural and individual differences in conceptual knowledge affect how expressions are interpreted (Lee et al., 2012). These behavioral and perceptual studies bolster the constructionist claim that emotions are actively constructed by integrating contextual and conceptual information, not simply “read” from invariant facial signals.

There is increasing evidence supporting this involvement of domain-general networks in emotion perception. While multivariate pattern analysis (MVPA) studies have shown that both localized and distributed neural patterns can predict emotional states (Kragel and LaBar, 2016), findings remain inconsistent, especially in the prefrontal cortex (PFC) (Westgarth et al., 2021; Bendall et al., 2016). Some fNIRS studies report increased PFC activation during facial emotion recognition (e.g., in the ventral and medial PFC), others find decreased or no significant changes in oxygenated hemoglobin (HbO) levels. Even studies using similar facial expression tasks report varying activation patterns depending on the specific emotion or cortical region involved. For instance, happy and fearful faces have been associated with increased right PFC activation, whereas sad faces tend to elicit decreased activation in the left PFC. These mixed findings echo fMRI research, which implicates a wide network, including the medial PFC, amygdala, fusiform gyrus, superior temporal sulcus, and insula in emotion perception, with specific emotions such as anger, disgust, and sadness engaging distinct cortical and subcortical areas. These findings underscore the complexity of emotion processing and highlights the need for more nuanced investigations of how different emotional expressions are represented in the brain.

## 1.2 Real vs. Virtual (Avatar) Face Perception

The increasing use of avatars has raised questions about how their facial expressions compare to real human faces. Avatars can be designed to mimic human facial expressions using the FACS, which demonstrates the efficacy of using FACS-based design principles to create reliable virtual human facial expressions (García et al., 2020). Studies have shown that expressions of happiness, anger, fear, and other basic emotions can be accurately interpreted from both static and dynamic virtual avatars (Faita et al., 2015; Dyck et al., 2008). However, in some cases, avatars may convey emotional expressions more or less effectively than real human faces. Disgust is particularly challenging to convey using current avatar technology, while it has been found that virtual expressions of sadness and fear are recognized more accurately than their natural face counterparts (Dyck et al., 2008). There are guiding principles for designing avatars that can effectively convey emotional expressions as well as real faces, as it has been found that people are generally less accurate at recognizing emotions from robotic faces compared to human faces (Hortensius et al., 2018). However, virtual agents can be as effective as humans in conveying emotions, particularly when their facial muscle movements are clearly depicted. This work highlights the potential for avatars to convey facial/emotional expressions effectively, but it also raises questions about how these virtual faces are processed in the brain compared to real human faces.

A growing body of affective and cognitive neuroscience research suggests that virtual faces, while often processed like real faces, can still elicit distinct neural responses due to differences in perceived authenticity, dynamicity, and realism. Since humans are highly attuned to perceiving real human faces, viewing avatars may engage different perceptual and neural processes, potentially leading to altered brain activity (De Borst and De Gelder, 2015). For instance, fearful human expressions elicit significantly stronger neural responses than fearful avatar expressions in regions including the posterior and

anterior superior temporal sulcus, anterior insular cortex, posterior cingulate cortex, and ventral anterior cingulate cortex, with particularly strong effects observed in both the left and right superior temporal sulcus and inferior frontal gyrus (Kegel et al., 2020). In contrast, neutral human and avatar expressions did not differ significantly. Using EEG, and the same dynamic stimuli as Kegel et al. (2020), it was found that avatar faces elicit significantly stronger reactions than the real faces for theta and alpha oscillations (Sollfrank et al., 2021). This may be affected by the degree to which the avatar resembles the observer's own appearance and habitual expressions, as observers' responses to avatar facial expressions are modulated by the degree to which the avatar resembles their own appearance and habitual expressions (Park et al., 2021). It is important to note, findings from studies using avatars and those using real human faces may not always be directly comparable and should be interpreted cautiously.

These perceptual discrepancies may partially stem from the so-called "uncanny valley" phenomenon (Mori et al., 2012), wherein highly realistic but imperfect virtual faces evoke a sense of unease or cognitive dissonance in observers. When watching semirealistic computer-animated film characters, it was found that characters perceived as more realistic were rated as more 'eerie', compared to more cartoonish characters (Kätsyri et al., 2017). The N170 is an event-related potential (ERP) component, commonly investigated in EEG studies, that is typically observed over occipitotemporal scalp regions and is associated with the early perceptual processing of faces. There is a non-linear modulation of EEG responses to the realness of face images, suggesting that the brain's processing of facial stimuli is sensitive to their perceived authenticity (Chen et al., 2024). This sensitivity to realism is further supported by findings that the N170 component is modulated by the degree of realism in facial expressions, as across six face-stylization levels ranging from abstract to realistic, it was found that the N170 was generated more occipitally for abstract/virtual faces than for real faces (Schindler et al., 2017). These findings suggest that small deviations from typical human facial expressions can lead to

altered neural processing.

Despite the rich EEG and fMRI evidence, there remains a notable gap in our understanding when it comes to fNIRS. To date, only a handful of studies have utilized fNIRS in avatar emotion research, and these have typically focused on bodily expressions (e.g., expressive gait), not facial emotion processing. For instance, cortical responses to emotional body movements expressed by faceless avatars were examined, revealing increased HbO in occipito-temporal and temporo-parietal areas, especially in response to negative emotions, during tasks requiring conscious emotion recognition (Schneider et al., 2014). The only study to examine facial emotion processing in avatars used fMRI, dynamic stimuli, and only utilized two emotions, fear and neutral (Kegel et al., 2020). Since there is an absence of fNIRS-based studies of facial emotional perception in avatar form, this thesis aims to fill this gap by investigating how the brain processes emotional expressions in both real and virtual faces using fNIRS. We examine the differences across the full set of basic emotions, not just fear and neutral, and use virtual static facial expressions to allow for a more controlled comparison with static real faces.

### 1.3 Functional Near-Infrared Spectroscopy (fNIRS)

fNIRS is a non-invasive neuroimaging technique that measures brain activity by detecting changes in Blood Oxygenation Level Dependent (BOLD) signals, which are associated with neural activity, similar to functional magnetic resonance imaging (fMRI). fNIRS works by shining near-infrared light (760-850nm) through the scalp and measuring the amount of light that is absorbed by oxygenated (HbO) and deoxygenated hemoglobin (HbR) in the brain. This is possible through the Modified Beer-Lambert Law, which relates the concentration of hemoglobin to the absorption of light (Kocsis et al., 2006). It is substantially more portable and cost-effective than MRI, tolerates moderate participant movement, and can be deployed in more ecologically valid or naturalistic settings

(Yücel et al., 2017). Temporal resolution is moderate, on the order of seconds, which, although inferior to EEG’s millisecond fidelity, remains sufficient to capture the hemodynamic responses associated with emotional and cognitive processes. Despite these advantages, fNIRS remains limited to superficial cortical regions; it lacks sensitivity to deeper subcortical structures such as the amygdala or insula, which play key roles in emotion processing (Sato et al., 2004). Its spatial resolution is also lower than fMRI’s, and signal quality can be influenced by factors like hair density and skin pigmentation (Holmes et al., 2024). Beyond systemic noise, fNIRS signals can also be affected by light in the recording environment and interference from participant hair; these issues can be minimized through careful preparation and room setup. These limitations are mitigated through methodological refinements, such as high-density optode arrangements, short-separation channels (Scholkmann et al., 2014), and motion correction techniques (Fishburn et al., 2019; Bergmann et al., 2023).

In analyzing our fNIRS data, we focused on two complementary approaches: the General Linear Model (GLM) and functional connectivity. The GLM is concerned with the magnitude of brain responses in specific regions, i.e., how much a brain area ”lights up” during a task, whereas functional connectivity looks at the relationship between different brain regions over time, regardless of their absolute activation levels. These methods provide a comprehensive view of how the brain processes emotional expressions, both in terms of localized activation and the interactions between different regions.

We used the GLM to estimate cortical activation in response to emotional facial expressions. In this approach, the task design (e.g., when a participant sees a face) is modeled using a boxcar or impulse function and convolved with a canonical hemodynamic response function (HRF), producing a predictor of the expected signal. The GLM then estimates how well this model fits the actual fNIRS signal, allowing us to identify brain regions that responded to different conditions (Tak and Ye, 2014). This approach is particularly well-suited to fNIRS data, which is often noisy, correlated across channels,

and influenced by physiological rhythms. The GLM helps to account for these complexities and isolate condition-specific activation (Huppert, 2016). We used the GLM to compare brain responses across emotional categories (e.g., anger, happiness), between real and virtual facial expressions, and their interaction.

In addition to activation analysis, we examined functional connectivity, which allowed us to explore how different brain regions process these faces and emotions in relation to each other. Unlike the GLM, which focuses on localized activity, functional connectivity examines temporal correlations between signals across channels. Functional connectivity can be assessed using various methods, including coherence, phase-slope index, and Granger causality (Bastos and Schoffelen, 2016). We focused on Wavelet Transform Coherence (WTC), which is the most commonly used method in fNIRS connectivity research, having been used in at least 90 studies to date (Hakim et al., 2023). WTC involves convolving the fNIRS signal with a wavelet function (such as the Morlet wavelet) to assess the strength and phase relationship of shared frequency components between brain regions in the time-frequency domain. This is particularly useful for fNIRS, where signals are non-stationary and vary across time. WTC enabled us to detect both in-phase and out-of-phase relationships between channels, helping us distinguish genuine neural connectivity from systemic noise. This method allows us a different perspective on how the brain processes emotional expressions, focusing on the relationships between regions independent of the magnitude of their activation.

## 1.4 Objectives and Hypotheses

Critically, functional near-infrared spectroscopy (fNIRS) demonstrates strong sensitivity to the PFC, a brain region heavily implicated in the perception, interpretation, and regulation of emotion (Westgarth et al., 2021; Bendall et al., 2016). Although prior studies have independently examined facial emotion perception and avatar realism, very few have

explored their interaction within the same neuroimaging paradigm, and even fewer have used fNIRS to do so. To our knowledge, no existing research has directly compared neural responses to emotional expressions in real versus virtual faces using a fully crossed, within-subject fNIRS design that systematically examines all basic emotions. This gap limits our understanding of how face realism and emotion interact to shape cortical activation patterns and functional connectivity during social perception. Accordingly, this thesis hypothesizes that: (1) there will be significant differences in brain activation patterns and functional connectivity profiles when viewing virtual faces compared to real faces, and (2) distinct emotional expressions will elicit unique neural activation and connectivity patterns. Given the novelty of this approach and the full range of emotions considered, we do not make specific *a priori* predictions about the exact nature of these differences, as they may vary based on emotional content and face realism. Addressing this gap will deepen our understanding of emotional cognition in the digital age and inform the design of emotionally expressive avatars for applications in education, mental health, and human-computer interaction.

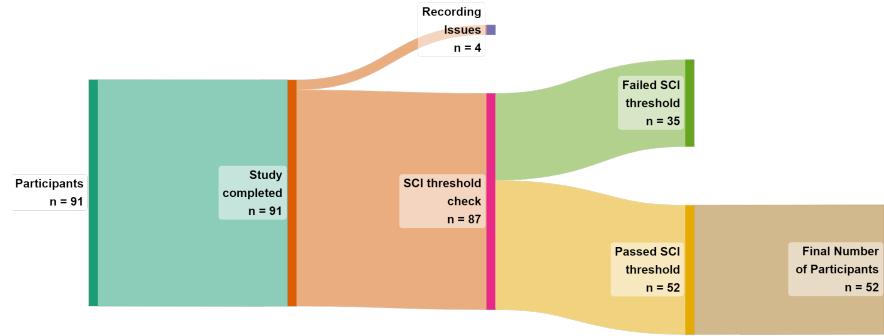
# Chapter 2

## Methodology

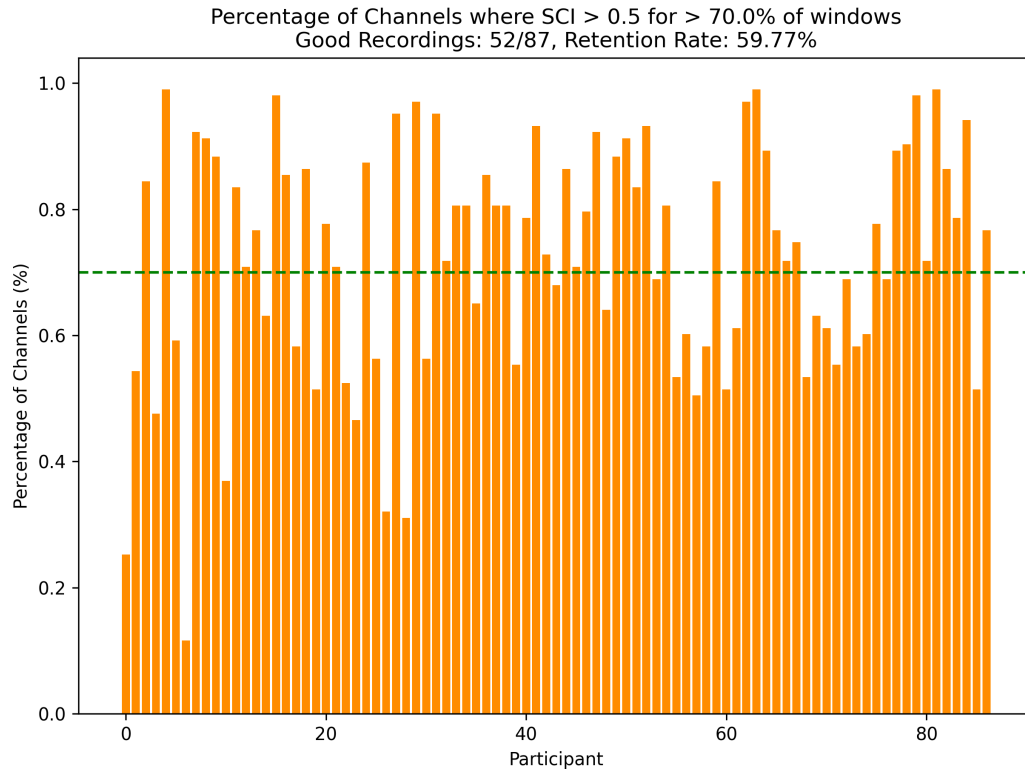
### 2.1 Participants

Ninety-one participants were recruited from Ontario Tech University's undergraduate student body through SONA. Participation flow is illustrated in Figure 2.1a. Four participants were removed due to equipment recording issues. Participants were then screened on inclusion criteria for a) task attention, and b) fNIRS signal quality. For attention, participants were required to achieve  $\geq 60\%$  accuracy on the behavioral memory task (chance accuracy = 50%) to ensure sufficient engagement. One participant failed to meet this criterion. The remaining 87 participants (69 females and 18 males,  $M = 21.09$ ,  $SD = 5.91$ , range = 17 to 51) were analyzed in the behavioral memory task. For neural analyses, signal quality of remaining 87 participants by computing the Peak Spectral Power (PSP) and the Scalp Coupling Index (SCI) (Pollonini et al., 2016). Measures were calculated using a 5-second sliding window across all channels (Bulgarelli et al., 2025; Hernandez and Pollonini, 2020). fNIRS inclusion criteria were: 1) PSP  $> 0.1$  and SCI  $> 0.5$  for more than 70% of the windows in a single channel, labelled "good signal quality" (Holmes et al., 2024), and 2)  $> 70\%$  of the channels for a single participant were marked as "good". Thirty-five participants failed to meet these criteria, illustrated in Figure 2.1b,

and were removed prior to data analysis. The final sample consisted of 52 participants (39 females and 13 males,  $M = 21.62$ ,  $SD = 6.67$ , range = 17 to 51).



(a) Sankey diagram showing the flow of participants through each stage of inclusion/exclusion in the study.



(b) Percentage of Channels where  $SCI > 0.5$  for  $> 70\%$  of the windows. The green dashed line represents the threshold of 70% of windows that each participant must meet to be included in the analysis.

Figure 2.1: (A) Participant inclusion flow diagram. (B) SCI signal quality inclusion threshold.

## 2.2 Stimuli and apparatus

### 2.2.1 Stimuli

One hundred and forty images of facial expressions from the racially diverse affective expression (RADIATE) and UIBVFED datasets were used ([Conley et al., 2018](#); [Oliver and Amengual Alcover, 2020](#)). The RADIATE contains perceptually validated images of racially and ethnically diverse participants, aged 18-30 years old, each expressing 16 different emotions. The UIBVFED dataset contains a set of 20 virtual characters that are also ethnically diverse, aged 20-80 years old expressing 32 emotions. The UIBVFED facial expressions were created using blendshapes, a tool that represents and manipulates clusters of facial landmarks similar to that of facial action units (AUs). Then adult models (5 males and 5 females) from each dataset were identified and matched between-sets on face shape, sex, skin tone, and hair colour. Images of each model expressing seven emotions (anger, disgust, fear, happiness, sadness, surprise, neutral) were selected. Expressions were selected for each model, that closely align with Ekman's 6 basic emotions + neutral ([Ekman and Friesen, 1971](#)). UIBVFED images were cropped to the same size as RADIATE images.

### 2.2.2 Apparatus

Participants were tested individually in a quiet dedicated testing room. Stimuli were presented on a Dell U2415 24-inch monitor at 1920x1200 60Hz. Participants were seated in a comfortable non-movable chair, with the monitor placed at eye level. Stimuli were presented using PsychoPy3 Experiment Builder (v2024.1.5) ([Peirce et al., 2019](#)). Participant brain activity was recorded using Aurora fNIRS while participants completed the task. fNIRS data was collected using two NIRSport2 systems (NIRx Medical Technologies, Berlin, Germany). Each NIRSport2 system was equipped with 16 source and 16 detector optodes, and daisy-chained together for a high density 32x32 optode configuration. Each

neighboring pair of source and detector optode is referred to as a channel, resulting in a total of 103 HbO + 103 HbR channels (plus 16 short distance channels). The average distance between source and detector optodes was 30 mm, and 7mm for short distance channels, which were placed on a flexible fNIRS head cap (NIRScap) 58 cm in circumference. The optodes were arranged in a high density 32x32 montage with one bundle of short distance channels, as shown in Figure 2.2. This montage was designed to cover a maximally large area of the brain, given increasing evidence that emotion processing is not localized to specific discrete areas of the brain, rather distributed across the brain (Lindquist et al., 2012). The fNIRS cap and optodes were positioned following the 10-20 international coordinate system. Light was emitted at 760 nm and 850 nm wavelengths, and the sampling rate was approximately 6.105 Hz.

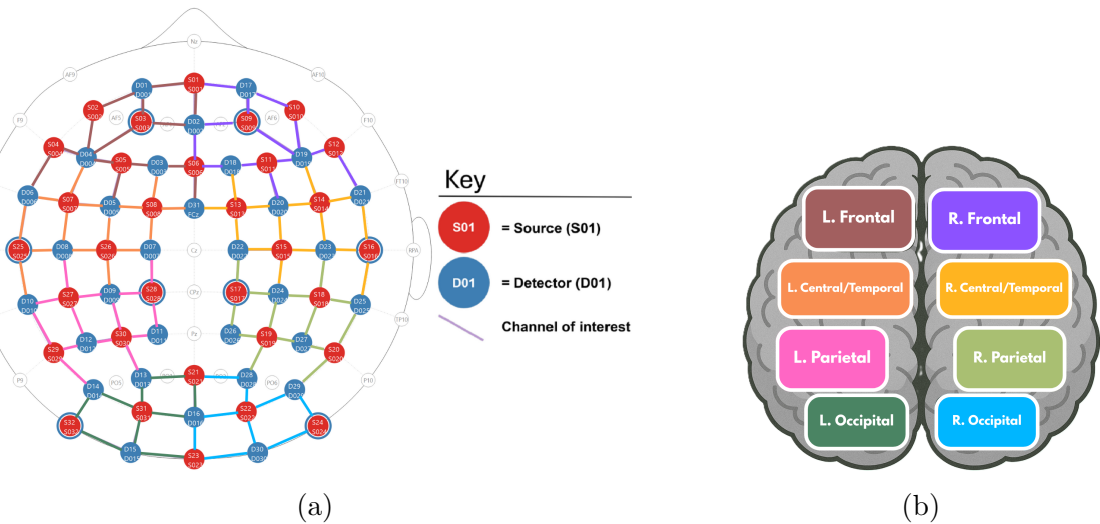


Figure 2.2: (a) Depictions of the high density 32x32 optode montage. Red circles represent sources, blue circles represent detectors, the colored lines represent channels, and blue rings around sources represent the locations of the 8 short distance detectors. The colors of the channels represent the regions of interest (ROI's) that the channels were grouped into. (b) Brain region map, showing the regions of interest (ROI's) that the channels were grouped into for certain analyses.

## 2.3 Design and procedure

### 2.3.1 Design

A full-factorial Face-type (2 levels: Real, Virtual)  $\times$  Emotion (7 levels: Anger, Disgust, Fear, Joy, Sadness, Surprise, Neutral)  $\times$  Model (4)  $\times$  Sex (2 levels: Male, Female)  $\times$  Repetition (4) experimental design was used, with each participant presented with 448 images. Stimuli were blocked and counterbalanced by Face-type and Emotion. Within each of the 56 Face-type-Emotion Blocks, participants were presented with 8 distinct model faces (4 male, 4 female).

### 2.3.2 Procedure

Following consent and briefing, participant head size was measured and a size-appropriate fNIRS cap fitted. A signal optimization routine was then run within Aurora fNIRS to optimize participant channel signal levels. This routine worked by increasing source brightness in a stepwise manner, until the optimal signal levels for all channels was reached. Following optimization, participants were told that they would be presented with a series of facial expression images and asked to identify whether a probe face matched one of the faces they saw in the preceding block. Room lights were then switched off to avoid interference with the fNIRS cap, and participants were monitored from an adjacent room with a live camera feed.

The experiment began with instructions presented on screen. The trial timeline, shown in Figure 2.3, consisted of three main epochs: fixation cross, block presentation, and participant feedback. Each Block began with a fixed cross presented for 16 seconds, followed by 8 facial images. Facial images were each presented for 1.5 seconds, with a 250-750 ms ( $M=500$  ms) interstimulus interval (ISI) between each face. To maintain participant attention, participants completed a memory task after each block. In the task, participants were presented with a model image with the same emotional expression as

the rest of the block's images, and asked if the model was shown in the preceding block of 8 faces, with feedback provided using the keyboard (y/n). The probe face has a 50% chance of either being in the previous block or not. The experiment continued after seven seconds if no feedback was provided (the distribution of block missed responses is shown in Appendix C.1). Participants were given a break every seven blocks, and prompted to enter the space bar when they are ready to continue the experiment. After the experiment was completed, the experimenter(s) entered the room, removed the fNIRS cap, and the participant was debriefed about the experiment. Participation in the experiment took approximately 35 minutes.

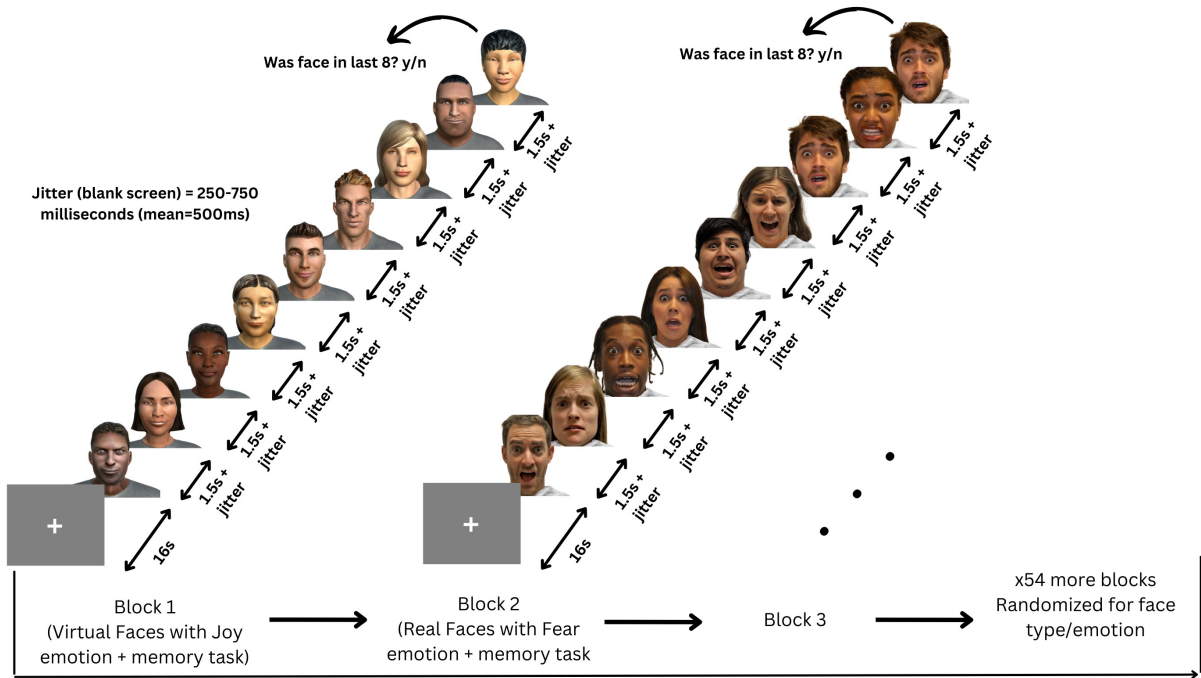


Figure 2.3: Participants viewed 56 blocks of 8 faces, each block being either all real or all virtual faces. Every face in a block displayed the same emotional expression, one of: anger, disgust, fear, happiness, sadness, surprise, neutral.

## 2.4 Analyses

All fNIRS data was preprocessed and analyzed with Python 3.11.9 using MNE (version 1.9.0) (Gramfort et al., 2013) and MNE-NIRS (version 0.7.1) (Luke et al., 2021), which

used the Nilearn package (version 0.9.2). Data were analyzed with a General Linear Model (GLM), followed by a functional connectivity analysis. The memory task was analyzed in Python using the statsmodels package (version 0.14.4) ([Seabold and Perktold, 2010](#)). The data generated during this study has been made publicly available on the Open Science Framework (OSF) [here](#).

### 2.4.1 fNIRS preprocessing

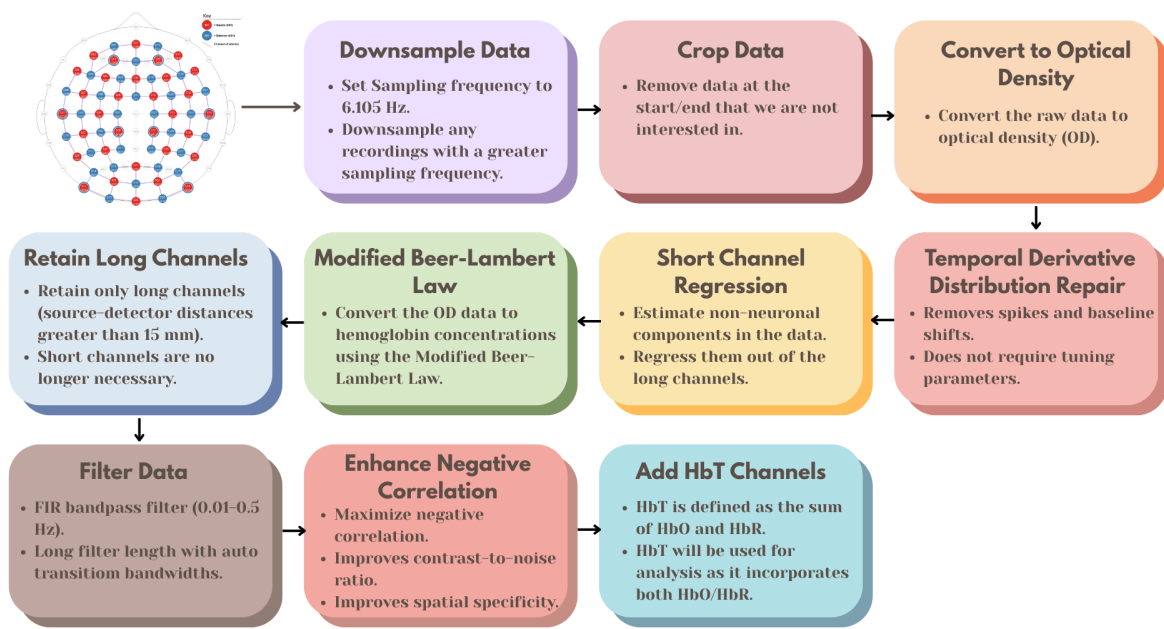


Figure 2.4: Preprocessing steps for fNIRS data, from the raw data to the fully processed data.

The preprocessing steps for the fNIRS data, as shown in Figure 2.4, were as follows:

- 1) Downsample the data if the sampling frequency is greater than 6.105 Hz, the initial two datasets were sampled higher than 6.105 Hz, and the sampling frequency should be consistent across all datasets.
- 2) Crop the data to the first and last annotation. This gets rid of the extra data at the beginning and end of the recording that are not of interest.
- 3) Convert the raw data to optical density.
- 4) Apply temporal derivative distribution repair to the OD data ([Fishburn et al., 2019](#)). TDDR is effective at removing spikes and baseline shifts.

shifts from the data. 5) Apply short channel regression to the OD data ([Scholkmann et al., 2014](#)). Short channels are used to estimate the superficial hemodynamics (non-evoked/extracerebral/systemic components) in the data, and then regress it out of the long channels ([Tachtsidis and Scholkmann, 2016](#)). 6) Convert the OD data to hemoglobin concentrations using the modified Beer-Lambert law. The MBLL relates the change in light attenuation to the change in hemoglobin concentration of chromophores in the tissue ([Kocsis et al., 2006](#)). 7) Retain only long channels (source-detector distance > 15 mm). Since the short channels have already been regressed out, it is no longer necessary to keep them in the data. 8) This FIR bandpass filter extracts signal components in the 0.01-0.5 Hz range, it uses a long filter length (2015 samples) with automatically determined transition bandwidths by MNE-Python ([Pinti et al., 2019](#)). 9) Maximizes negative correlation between HbO and HbR ([Cui et al., 2010](#)). This method removes spikes, improves contrast-to-noise ratio, and improves spatial specificity of the data. 10) Add HbT (total hemoglobin) channels to the data. HbT is defined as the sum of HbO and HbR. Often, fNIRS studies will only use either one of HbO or HbR channels (more frequently HbO), leaving out one channel with no justification ([Kinder et al., 2022](#)). Therefore, HbT channels are chosen, as HbT makes use of both HbO and HbR channels, and using both hemoglobin species improves the inferences as to where activation occurs ([Hocke et al., 2018](#)).

Variable length epochs were created for each block of 8 faces, which were 14-18 seconds long (mean = 16s), depending on the ISI's (see [2.3.2](#)). Epochs were sorted by Face Type (Real, Virtual), and Emotion (Anger, Disgust, Fear, Happiness, Sadness, Surprise, Neutral), and their interaction. Baseline correction was applied to remove any constant or slowly varying offsets in the data. The data was annotated with the onsets and offsets of each block, along with the duration and condition of each block. Block data were then analysed using a GLM and Functional Connectivity analysis.

## 2.4.2 Activation magnitude with General Linear Model (GLM)

The General Linear Model (GLM) posits that the observed haemodynamic signal at each channel or Region of Interest (ROI) is a linear combination of task-related regressors convolved with a Hemodynamic Response Function (HRF), plus nuisance regressors (e.g., drift) and residual noise. Mathematically,

$$Y = X\beta + \epsilon, \quad (2.1)$$

where  $Y$  is the observed time series,  $X$  is the design matrix,  $\beta$  represents the parameters to estimate, and  $\epsilon$  denotes the residuals assumed to be Gaussian noise. Estimation is performed via ordinary least squares (OLS), yielding parameter estimates that quantify condition-specific activation amplitudes.

### Design Matrix

For each of the epochs, events are defined by their trial type (e.g., emotion or face type), and onsets/offsets relative to the procedure start, and duration. The design matrix is constructed using NiLearn's `make_first_level_design_matrix` by convolving a boxcar function (based on the event timing) with a canonical HRF, which is a model of the expected haemodynamic response to neural activity. The canonical HRF Statistical Parametric Mapping (SPM) (Friston, 2007) is chosen to model neurovascular coupling, this model captures the stereotypical rise and fall of the BOLD/fNIRS response. The cosine drift model was utilized, which incorporates discrete cosine transform (DCT) basis functions into the design matrix to model and remove low-frequency drifts. The selection of the high pass cutoff frequency is guided by the structure of the experimental design. The cutoff period is set to twice the duration of the longest inter-trial interval, and each fixation period between epochs (or blocks) is 16 seconds. Therefore, a cutoff period of 32 seconds (i.e., `high_pass=0.03125 Hz`) would be appropriate. This ensures that the drift

model does not remove task-related signal components that occur at frequencies higher than the cutoff (Luke et al., 2021). The design matrix  $X$  and preprocessed time series are fed into MNE’s `run_glm` function, which computes OLS estimates of  $\beta$  for each channel.

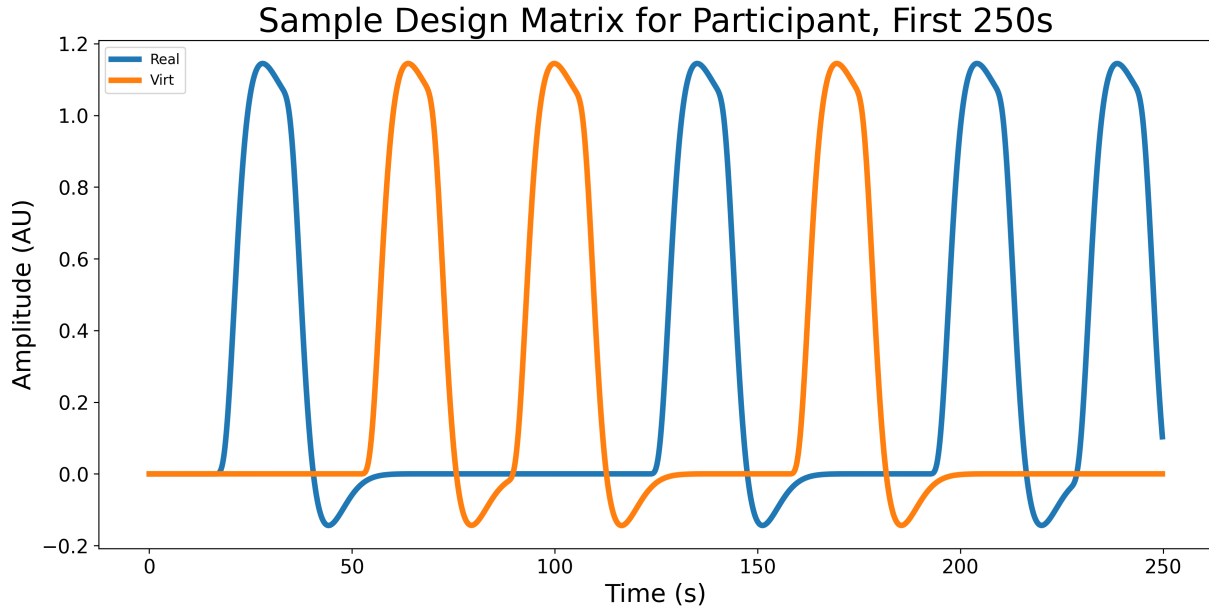


Figure 2.5: Sample design matrix for a single participant for the effect Face type, showing the first 7 blocks (250 seconds) of a single experiment. The design matrix is organized by condition (Blue for real, orange for virtual), this is the result of convolving the boxcar function with the canonical HRF SPM.

A two-way repeated measures GLM was conducted on participant’s HbT responses by Face-type (2 levels: Real, Virtual) and Emotion (7 levels: Anger, Disgust, Fear, Joy, Sadness, Surprise, Neutral). Pairwise contrasts were then computed between conditions to identify effects of interest.

### Contrast Computation

All pairwise contrasts were generated between conditions by constructing an identity contrast matrix over design columns. For each pair of conditions ( $A, B$ ), the contrast vector is defined as:  $c = e_A - e_B$ , where  $e_A$  and  $e_B$  are the respective design matrix columns for conditions  $A$  and  $B$ . Contrasts are computed using MNE’s `compute_contrast` function, which produces effect estimates and test statistics aggregated across channels. Since nu-

merous statistical tests are performed across channels and contrasts,  $p$ -values were FDR-corrected using the Benjamini-Hochberg procedure ([Singh and Dan, 2006](#)) with a family-wise error rate of  $\alpha=0.05$ .

### 2.4.3 Network mapping with Functional Connectivity Analysis

To characterize the temporal coordination between fNIRS channels during face and emotion processing, functional connectivity matrices were computed using a continuous wavelet transform (CWT)-based spectral connectivity approach. CWT decomposes signals into simultaneous time-frequency representations, providing an optimal framework for fNIRS connectivity analysis by accommodating the non-stationary, physiological nature of hemodynamic signals. The morlet wavelet, a gaussian function modulated by a sine wave, was picked as they are suited to capture both slow neural rhythms and faster systemic fluctuations in fNIRS data ([Reddy et al., 2021](#)). Wavelet-based approaches have been widely adopted in the fNIRS literature for connectivity and even artifact correction ([Bergmann et al., 2023; Hakim et al., 2023](#)). Coherence combines both phase and amplitude information into a single, normalized index, 0 (no coupling) to 1 (perfect coupling), and is a richer description of coupling than phase-only or amplitude-only metrics ([Bastos and Schoffelen, 2016](#)).

For each participant, MNE’s `spectral_connectivity_time` function was applied to compute time-resolved coherence across pairs of channels, the average of this was taken across epochs to obtain a single channel-by-channel connectivity matrix for each condition. Each participants’ connectivity matrix was then averaged across participants to obtain a group-level connectivity matrix for each condition. fNIRS hemodynamics predominantly fluctuate in very low frequencies (0.01-0.5 Hz) ([Reddy et al., 2021](#)). The frequency range was narrowed to five evenly spaced frequencies between 0.2-0.5 Hz due to short epoch length, this range still targets systemic and neurogenic oscillations while avoiding high-frequency noise ([Xu et al., 2017](#)). Averaging across these closely spaced fre-

quencies reduces data dimensionality, simplifying downstream statistical analyses without sacrificing sensitivity to coupling dynamics.

### Paired Sample t-tests

For each mode (Face type/Emotion), and pair of conditions (e.g., Joy vs. Fear), individual-level connectivity matrices were extracted by averaging across epochs to obtain symmetric channel-by-channel coherence matrices. Because coherence values are bounded between 0 and 1 and exhibit skewed distributions ([Miranda de Sá et al., 2009](#)), Fisher's r-to-z transform (`atanh`) was applied to each matrix element to normalize the data prior to parametric testing. Paired *t*-tests for each unique channel pair ( $i > j$ ) were then conducted across participants using SciPy's `ttest_rel`. This directly tests whether mean connectivity differs between conditions, leveraging the paired design to increase statistical sensitivity ([Hu et al., 2023](#)). Given the large number of channel-pair tests, and similar to the GLM analysis above in [2.4.2](#), *p*-values were FDR-corrected using the Benjamini-Hochberg procedure ([Singh and Dan, 2006](#)) with a family-wise error rate of  $\alpha=0.05$ .

### ROI Chord Plots

To distill high-dimensional channel-by-channel connectivity into interpretable inter-regional summaries, we mapped individual fNIRS channels onto anatomically defined ROI's. This includes left and right frontal, central/temporal, parietal, occipital regions of the brain as shown in Figure [2.2b](#), and the channels were grouped into these regions based on their location in the montage. Since multiple channels may map to the same pair of regions (e.g., several left central/temporal channels connecting to several right occipital channels), we calculated the sum of all significant channel-pair connections for each ROI pair (separately for positive and negative *t*-values). We then subtracted the negative sum from the positive sum, resulting in a single integer representing the net connectivity which was positive if the positive connections outweigh the negative ones, and vice versa.

We then took the top 15% percentile of each net connectivity value, and set the rest to zero, to show only the strongest connections between regions. The lines were then plotted using a chord diagram, with the line color indicating the direction of the net connectivity (positive or negative), and the line width indicating the magnitude of the net connectivity (the absolute value of the net connectivity).

### **Emotion Summary Ratio Plot**

To summarize the net connectivity between regions for each emotion, we calculated a ratio of positive to negative connections for each emotion pair. The ratio was calculated by taking the difference of the count of significant channels where the  $t$ -value was positive and the count of significant channels where the  $t$ -value was negative, and dividing it by the total number of significant channels for that emotion pair. This ratio provides a measure of the net connectivity across all ROI's for each emotion, with a positive ratio indicating that one emotion has a stronger net connectivity than the other, and a negative ratio indicating that the other emotion has a stronger net connectivity.

### **Region Summary Plot**

To summarize the net connectivity across all emotions for each region, we summed the number of significantly different channel pairs between each region pair across all emotions, disregarding the direction of the  $t$ -value. This provides a measure of the net connectivity across all emotions for each region, showing which regions are more connected across all emotions. The 3 regions with the highest and lowest number of significant channel pairs are marked, to emphasize the most/least connected regions across all emotions.

#### 2.4.4 Memory Task Analysis

Raw behavioral data captured from PsychoPy were preprocessed to identify participant keyboard responses. The total correct trials per participant were summed. Since each block of faces was either all real or all virtual, and all had the same emotional expression (as discussed in 2.3.2), each y/n response was labeled with Face type and Emotion. An OLS model was fit with accuracy (converted to numeric 0/1) as the dependent variable and categorical predictors for Face Type, Emotion, and their interaction. The goal is to determine the main effects of these two factors individually, as well as their interaction, on response accuracy. A two-way Type III ANOVA (via `sm.stats.anova_lm(model, typ=3)`) provided  $F$ -statistics and  $p$ -values for main effects and interaction. This version of the ANOVA is especially suitable when interactions are included in the model, as it calculates each effect after accounting for all other terms.

# Chapter 3

## Results

### 3.1 Neural activation magnitude

#### Responses to real and virtual faces

A main effect of Face type was reported, with pairwise contrasts revealing greater activation for virtual faces compared to real faces, as shown in Figure 3.1.

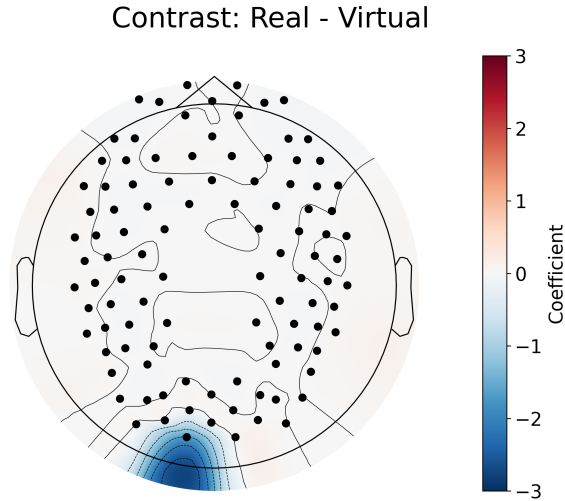


Figure 3.1: GLM contrast between real and virtual conditions which shows the differences in activation between the two conditions. Red signifies that condition 1 (real faces) has more activation in that area than condition 2 (virtual faces), while blue signifies that condition 2 (virtual faces) has more activation than condition 1 (real faces). The color bar on the right shows the coefficient of the contrast, which indicates the strength of the difference in activation between the two conditions.

## Responses to different facial emotions

Pairwise contrasts with Neutral (control) and other emotions revealed significant differences in activation across several brain regions (Figure 3.2). For instance, perceiving Anger, Fear, and Joy elicited less activity in the right occipital region than perceiving Neutral. Moreover, processing Joy was associated with less activity in the right parietal region, while processing Sadness produced less activity in the left frontal region relative to processing Neutral. These results indicate distinct neural activation patterns for each emotion when contrasted against the "baseline" Neutral condition, with most prominent differences in neural activity over the occipital region.

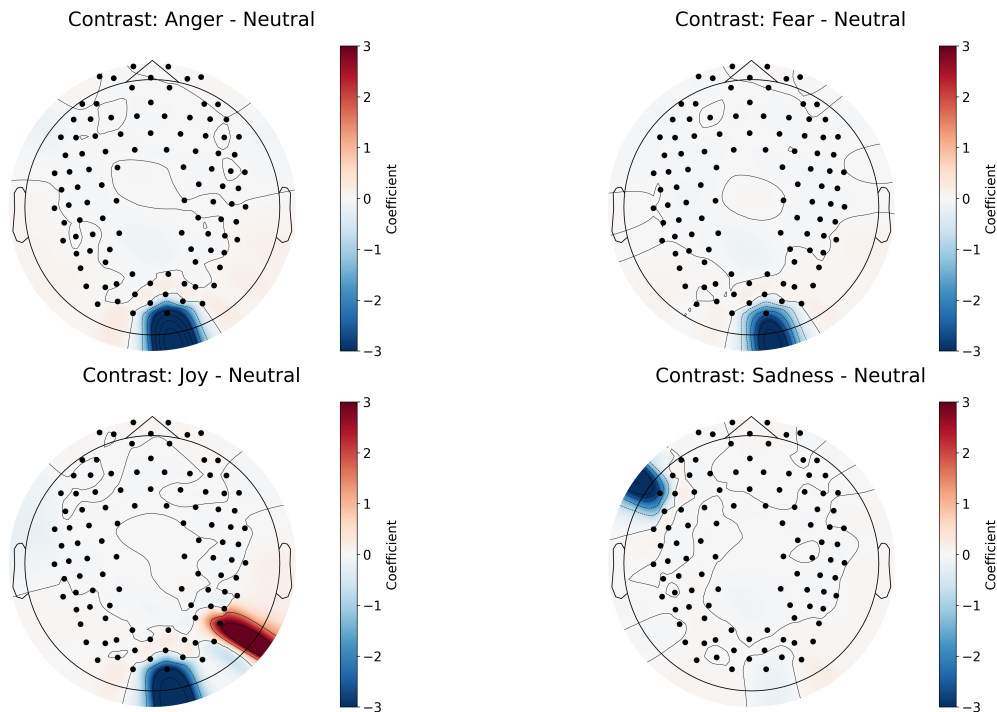


Figure 3.2: GLM results for the contrast between different emotions and neutral condition.

Interestingly, processing Surprise was most consistently different from processing other emotions (Figure 3.3). We found processing Surprise produced 1) more activity in the left central/temporal and right occipital regions relative to processing Disgust and Joy, 2) more activity in the right parietal region relative to processing Fear, 3)

more activity in the left frontal and right parietal regions relative to processing Sadness, and 4) more activity in the right parietal region and less activity in the right occipital region relative to processing Neutral. These findings suggest that Surprise is distinct from processing Neutral but also other emotions, with differences in neural activity more widespread that include central/temporal and parietal regions. All combinations of emotion contrasts were performed, significant differences were only found between Neutral relative to the other emotions, and between Surprise relative to the other emotions.

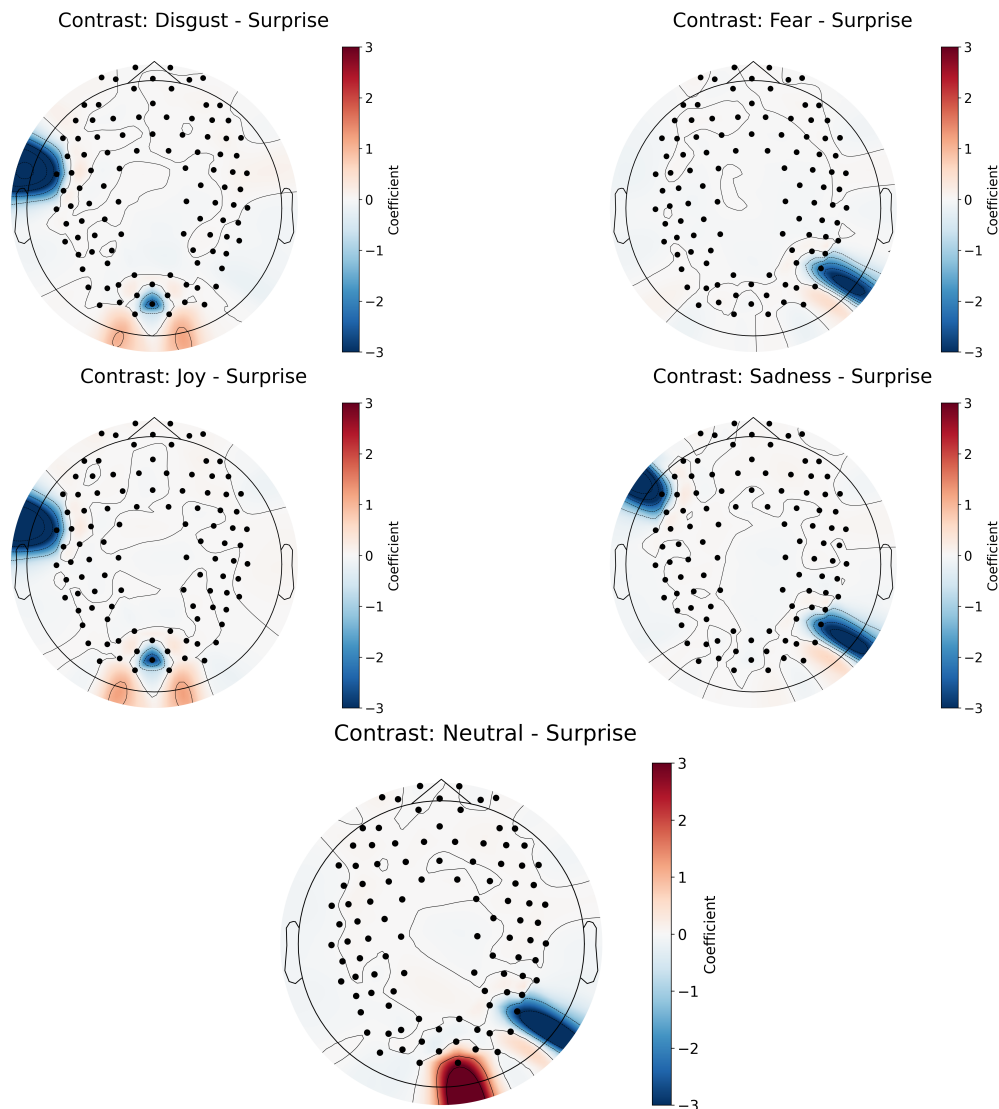


Figure 3.3: GLM results for the contrast between different emotions and surprise condition.

### Interaction in the responses to face type and emotion

The interaction of Real - Virtual within each emotion, as shown in Figure 3.4 revealed significant differences in occipital regions exclusively. Specifically, processing Disgust on real faces elicited greater activity in the right occipital region compared to processing Disgust on virtual faces, whereas the left occipital region showed the opposite pattern. Moreover, processing Joy and Neutral emotions on real faces also elicited greater activity in the occipital regions compared to processing the same emotions on virtual faces. We found processing Sadness on virtual faces produced more activity in the left occipital region for virtual faces compared to processing Sadness on real faces. These findings suggest that the neural response to emotional expressions is modulated by the realism of the face stimuli. The full table of the GLM contrasts for all main effects and interactions can be found in Appendix A.

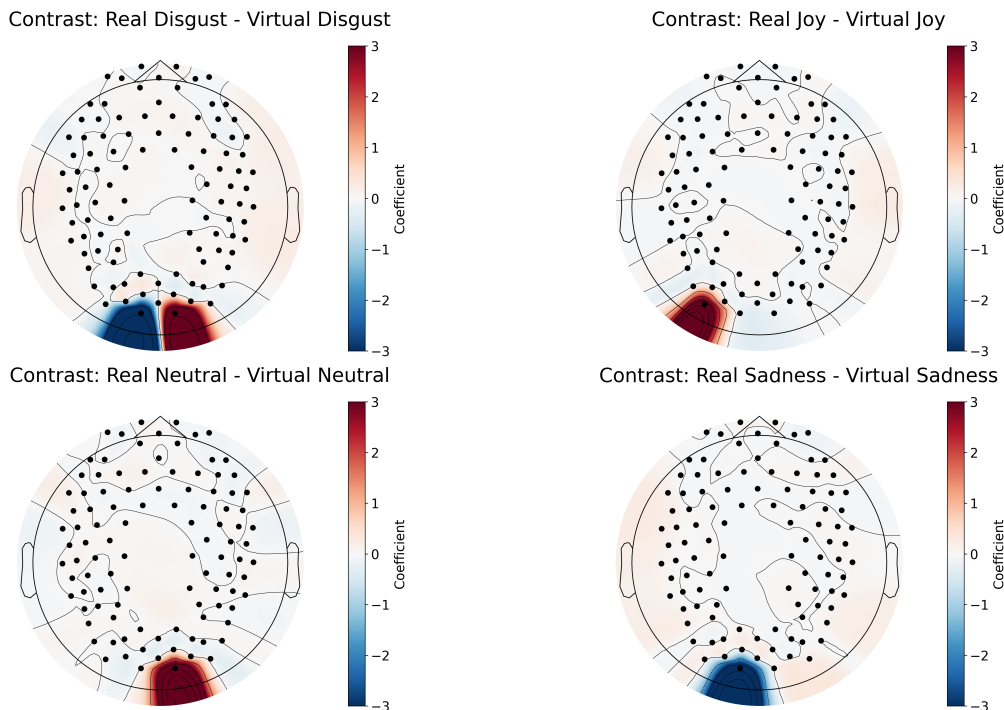


Figure 3.4: GLM results for the contrast between real and virtual conditions within each emotion.

## 3.2 Functional Connectivity Mapping

### Connectivity profiles of face type

The contrast comparing functional connectivity profiles in response to real versus virtual faces (as shown in Figure 3.5) revealed significant differences in connectivity across the brain. Processing real faces was associated with stronger connectivity predominantly between the left to right parietal, left frontal to left parietal, left central/temporal to left parietal, left central/temporal to right parietal, and the right central/temporal to left parietal regions, whereas processing virtual faces was associated with only slightly stronger connectivity between the left central/temporal to right frontal region.

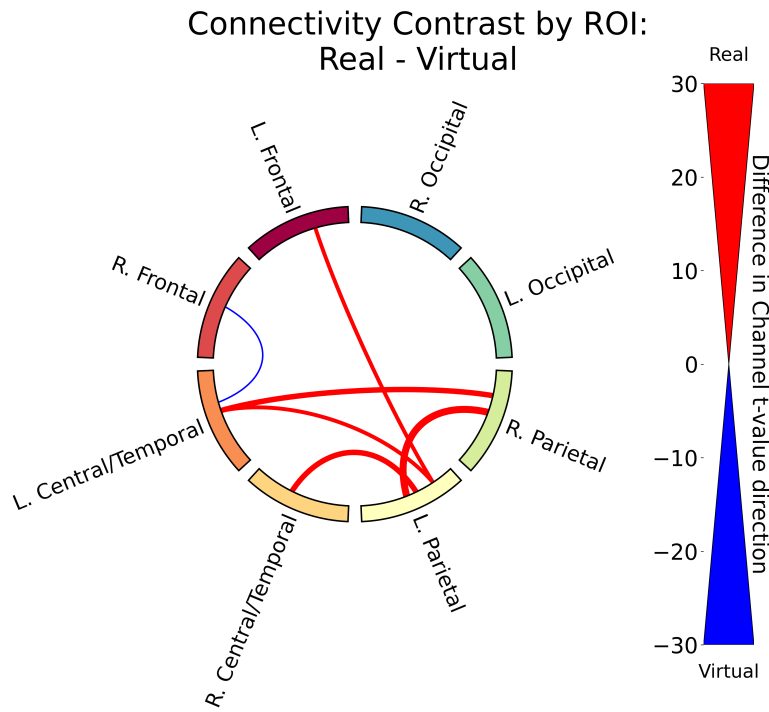


Figure 3.5: Functional connectivity results for the contrast between real and virtual conditions. The thickness of the lines represents the difference in the count of significantly different channel pairs between the two conditions. A red line signifies that real faces had more significant channels between those two ROI's where the  $t$ -value was positive, while a blue line signifies that virtual faces had more significant channels between those two ROI's where the  $t$ -value was negative. For clarity, only the top 15th percentile of connections (those with the most significant different channel pairs) are displayed for all functional connectivity contrasts.

### Connectivity profiles of facial emotion

We also found significant differences in functional connectivity in response to different emotions across all ROI's. A sample of the functional connectivity results which include only contrasts between Fear and the other emotions are plotted in Figure 3.6. We found the largest connectivity differences processing faces expressing Fear relative to Neutral faces, with significantly stronger connectivity between left central/temporal and right and left frontal, and right and left parietal. In general, we found processing faces expressing Fear produced significantly strong connectivity across the brain relative to faces expressing all other emotions, however this difference was weakest relative to processing angry faces. Interestingly most of the stronger connections emerge from the left central/temporal region, pointing to this region as a key area for processing Fear. The complete set of functional connectivity contrasts for all emotions can be found in Appendix B.

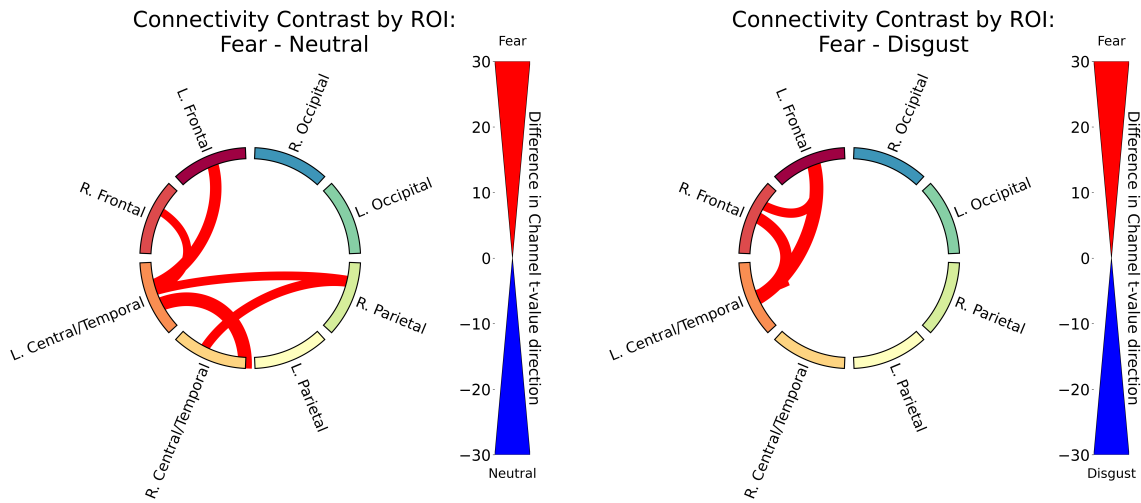
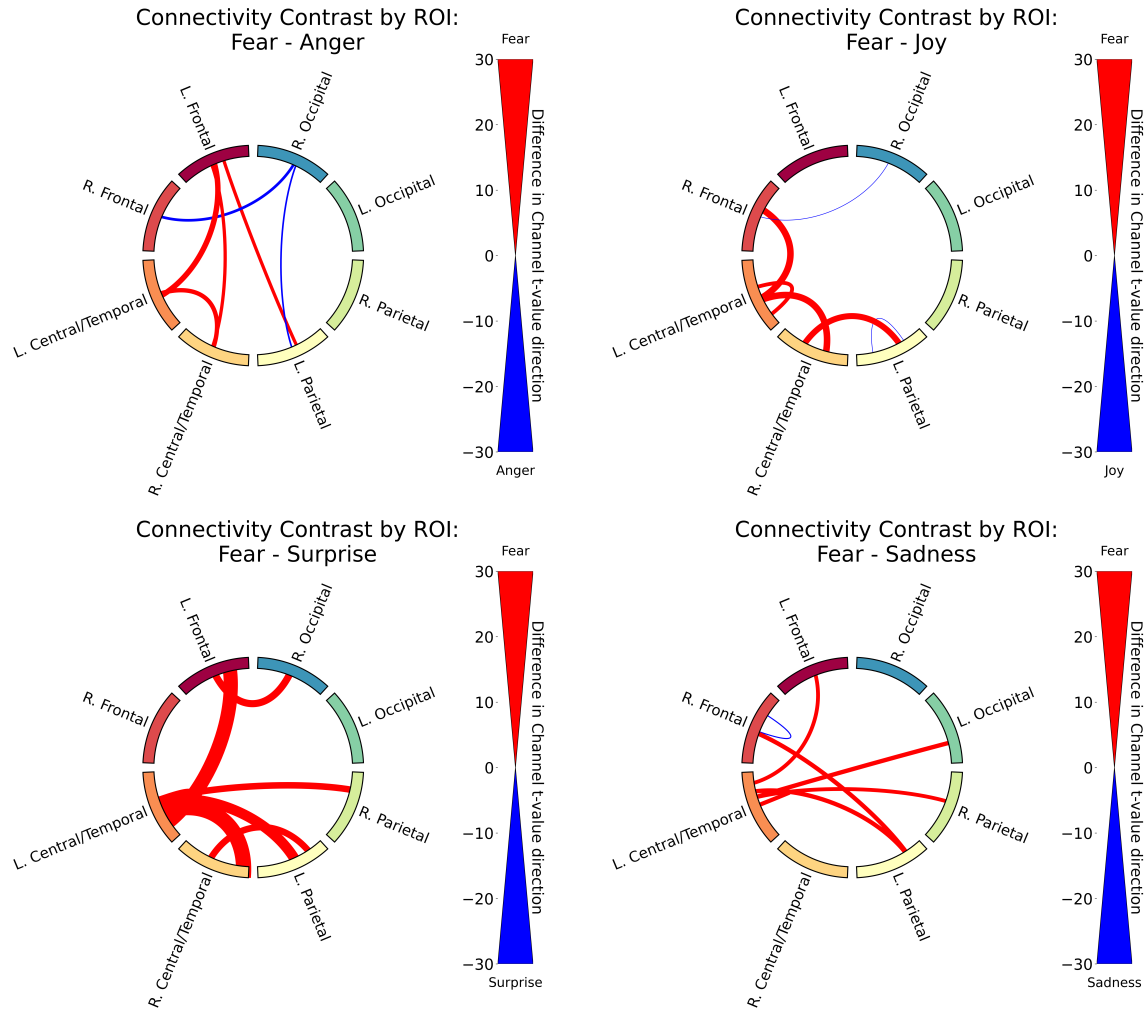


Figure 3.6: Functional connectivity results for Fear relative to Neutral and Disgust. (1/2)



Functional connectivity results for Fear relative to Anger, Joy, Surprise, and Sadness.  
(2/2)

To explore higher level patterns in Emotion, we calculated the ratio of significant channels, where the  $t$ -value was positive (red) or negative (blue) for each emotion pair, as shown in Figure 3.7. We found a cluster of emotions including Anger, Fear, and Joy, that reported stronger connectivity compared to the other emotions. Of these three, Fear > Anger > Joy, where the stronger functional connectivity for fearful and angry expressions suggests a neural prioritization of faces signalling potential threat, consistent with rapid threat-detection mechanisms, lining up with Figure 3.6. The other emotions (Neutral, Sadness, Surprise) had lower connectivity compared to Anger, Fear, and Joy, with Disgust having higher connectivity than Neutral.

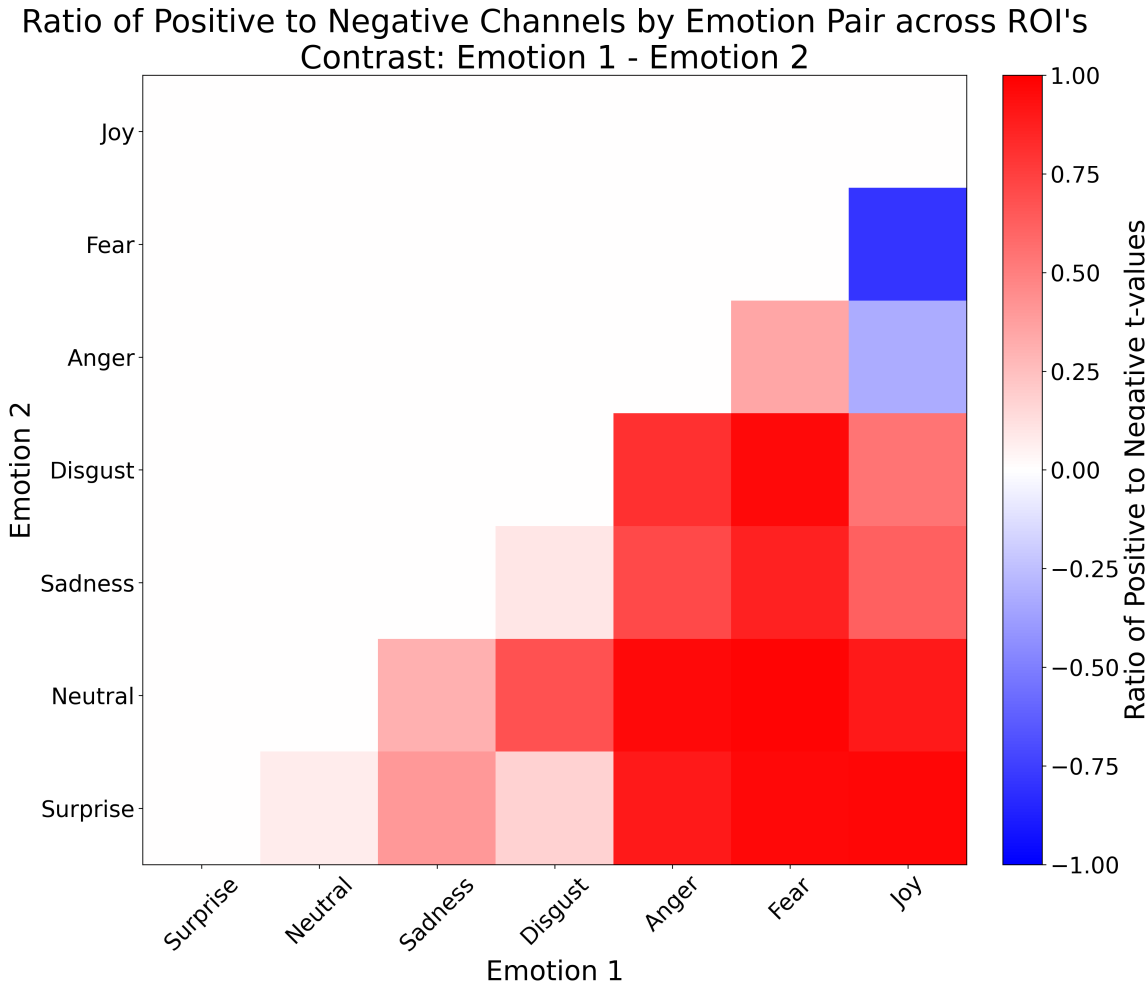


Figure 3.7: A heatmap summary of the functional connectivity results for the contrasts between different emotions across ROI's. Red signifies that emotion 1 had a higher ratio of significant channels where the  $t$ -value was positive, while blue signifies that emotion 2 had a higher ratio of significant channels where the  $t$ -value was negative. The ratio was calculated by taking the difference of the count of significant channels where the  $t$ -value was positive and the count of significant channels where the  $t$ -value was negative, and dividing it by the total number of significant channels for that emotion pair.

Next we sought explore higher-order patterns in brain regions connectivity. For this analysis, we generated a count of the number of statistically significant channels per region that differeed across emotion, and plotted as a heatmap as shown in Figure 3.8. The left central/temporal, parietal, and right central/temporal regions produced the greatest number of significant connections (marked with a caret), suggesting that these regions are more variable in their connectivity patterns across emotions. In contrast, left

and right occipital regions produced the fewest number of significant connections, marked with an asterisk, suggesting that the connectivity within and between these regions are similar in response to all emotions, and that neural indices that differentiate emotion processing likely occur in brain regions outside of the visual cortex.

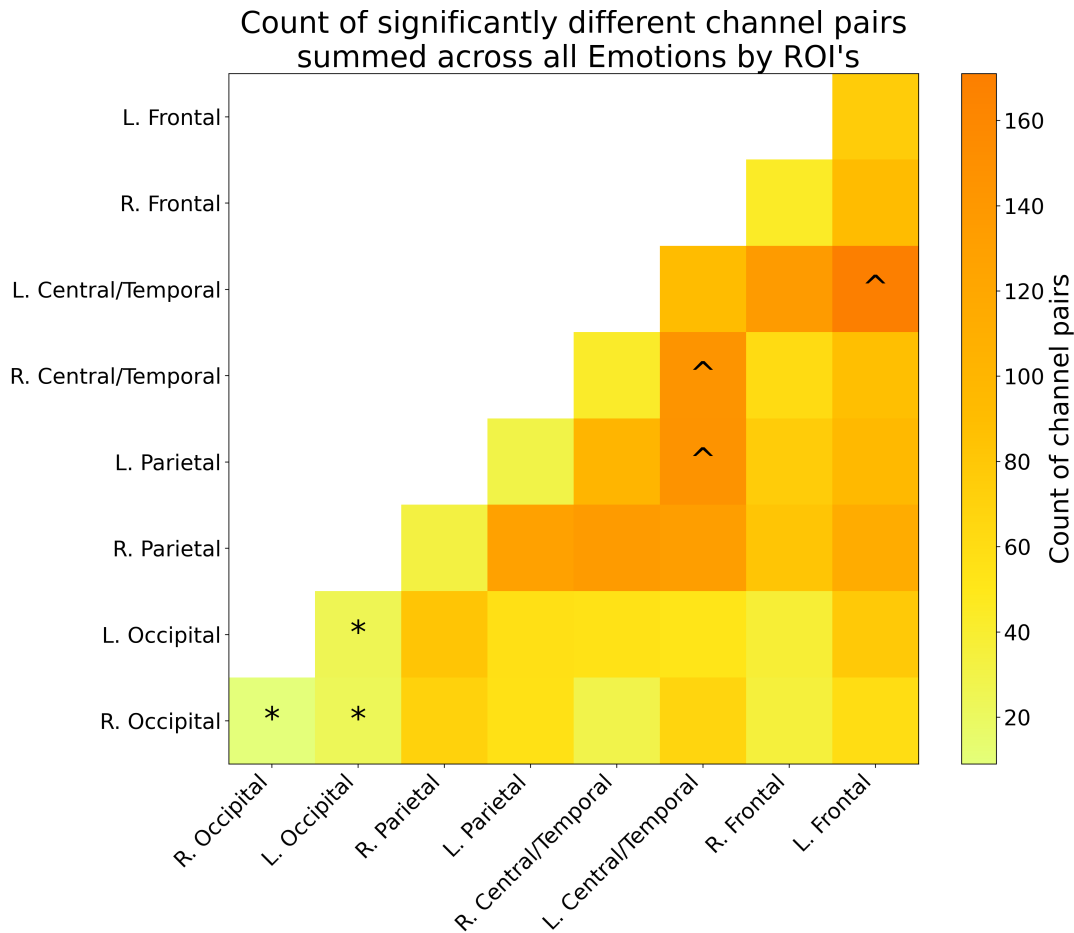


Figure 3.8: A heatmap summary of the number of significantly different channel pairs for each ROI summed across all emotions. The color bar on the right shows the number of significant channel pairs for each ROI, with brighter colors indicating a smaller number of significant channel pairs, and darker colors indicating a larger number of significant channel pairs. An asterisk (\*) was placed on the 3 ROI's with the least number of significantly different channel pairs to indicate that these ROI's are more synchronized with each other than any other pair of ROI's, regardless of the emotion. A caret (^) was placed on the 3 ROI's with the most number of significantly different channel pairs to indicate that these ROI's are less synchronized with each other than any other pair of ROI's, regardless of the emotion. Note that ROI's can have differences within them, as each ROI is made up of multiple channels, and the differences are calculated between channels within the same ROI.

### Differential Functional connectivity profiles in response to emotion across face type

The interaction of face type with emotion, Real - Virtual within each emotion (Figure 3.9) revealed significant differences in functional connectivity across the brain. We found that processing Anger on virtual faces elicited greater connectivity between the left frontal to right central/temporal, left frontal to right frontal, and within the left frontal region, compared to processing Anger on real faces. Processing Disgust on virtual faces elicited greater connectivity between the left frontal to left parietal, right frontal to left parietal, right frontal to left central/temporal, left frontal to left occipital, and right central/temporal to right parietal, compared to processing Disgust on real faces. Processing Fear on virtual faces elicited greater connectivity between many ROI's, particularly the left frontal to left occipital regions, between the left/right occipital regions, and between the left/right central/temporal and left/right occipital regions, compared to processing Fear on real faces. Processing Neutral on virtual faces elicited greater connectivity between the left frontal to right frontal, left/right frontal to right parietal, and left/right parietal regions, compared to processing Neutral on real faces. Processing Sadness on real faces elicited greater connectivity between the left frontal to right central/temporal, left central/temporal to right parietal, left central/temporal to right occipital, and right central/temporal to left parietal regions, compared to processing Sadness on virtual faces. Processing Surprise on real faces elicited greater connectivity between many ROI's, such as the left frontal to left/right central/temporal, left frontal to right parietal, left/right central/temporal to left/right parietal, and within the left/right central/temporal regions, compared to processing Surprise on virtual faces. Processing Joy on real faces elicited greater connectivity between the left/right central/temporal to right parietal, and within right parietal regions, whereas processing Joy on virtual faces elicited greater connectivity between the left central/temporal to left/right occipital regions. Overall, these results indicate that the effect of face type on functional connectivity varies by

emotion, with virtual faces generally eliciting greater connectivity for negative emotions (Anger, Disgust, Fear, Neutral), while real faces tend to elicit greater connectivity for positive emotions (Sadness, Surprise, Joy), and the specific brain regions involved differ across emotions. Like the GLM results, this indicates that the neural response to emotional expressions is modulated by the realism of the face stimuli. The full table of the functional connectivity contrasts for all main effects and interactions can be found in Appendix B.

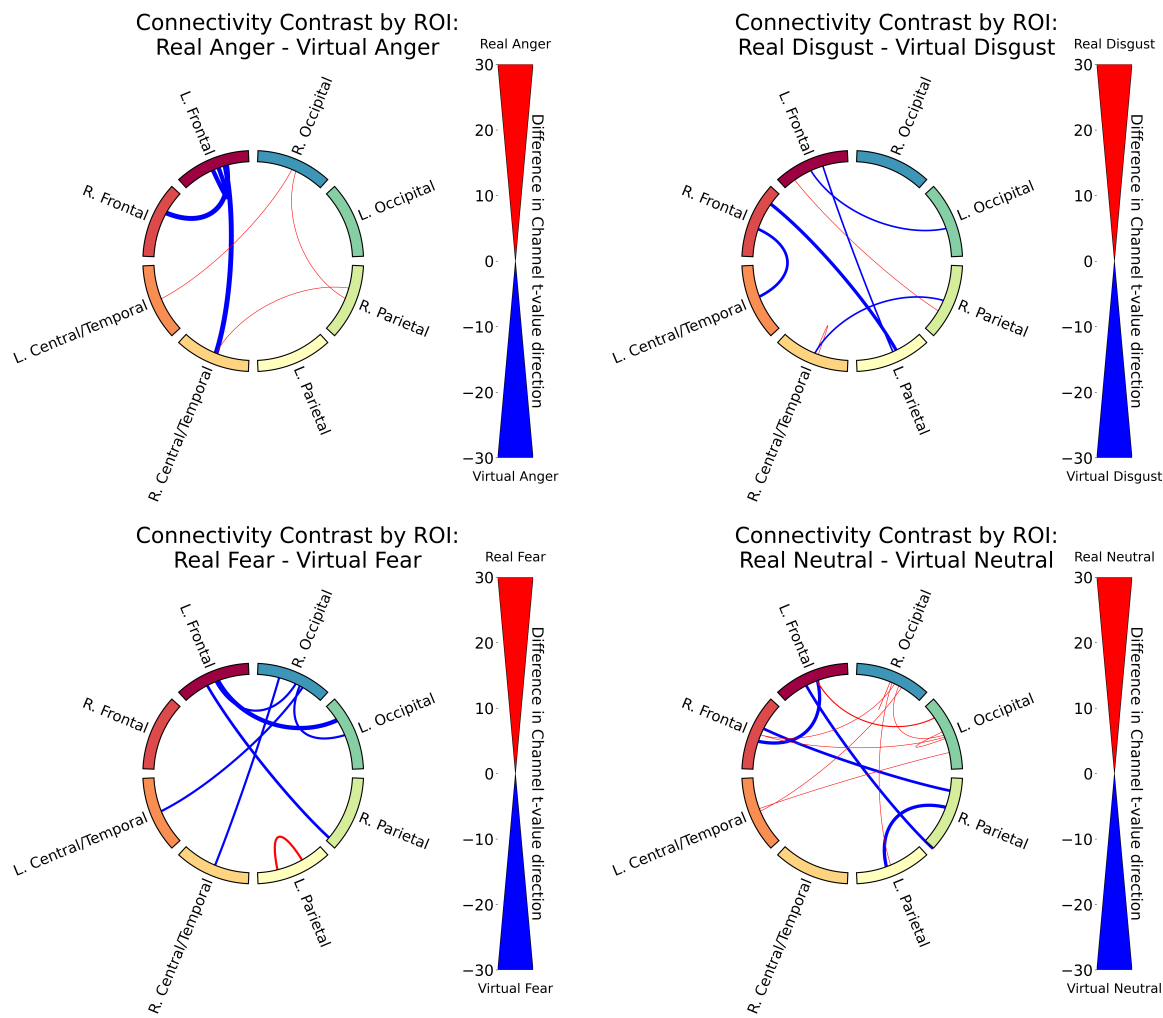
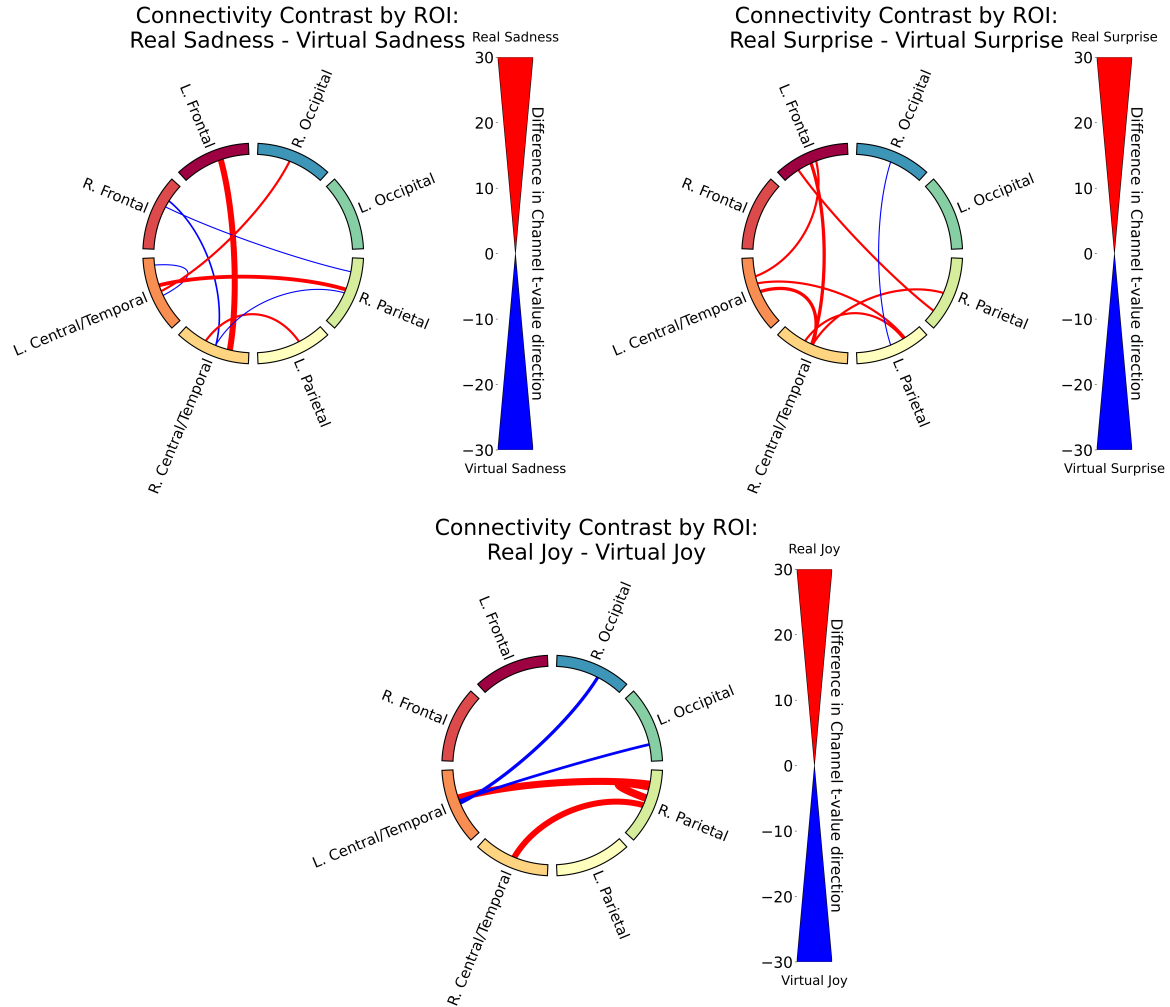


Figure 3.9: Functional connectivity results for the contrast between real and virtual conditions within each emotion. (1/2)



Functional connectivity results for the contrast between real and virtual conditions within each emotion. (2/2)

### 3.3 Memory Task Results

A two-way Type III ANOVA revealed a significant main effect of face type,  $F(1, 4802) = 7.96$ ,  $p = 0.0048$ , indicating that memory performance was higher for real faces compared to virtual faces, as shown in Figure 3.10. There was no significant main effect of emotion,  $F(6, 4802) = 0.83$ ,  $p = 0.55$ , nor a significant interaction between face type and emotion,  $F(6, 4802) = 0.46$ ,  $p = 0.84$ . These findings suggest that while the realism of the face influences memory performance, the specific emotional expression does not have

a significant impact on memory accuracy. The full ANOVA table is shown in Appendix C.1.

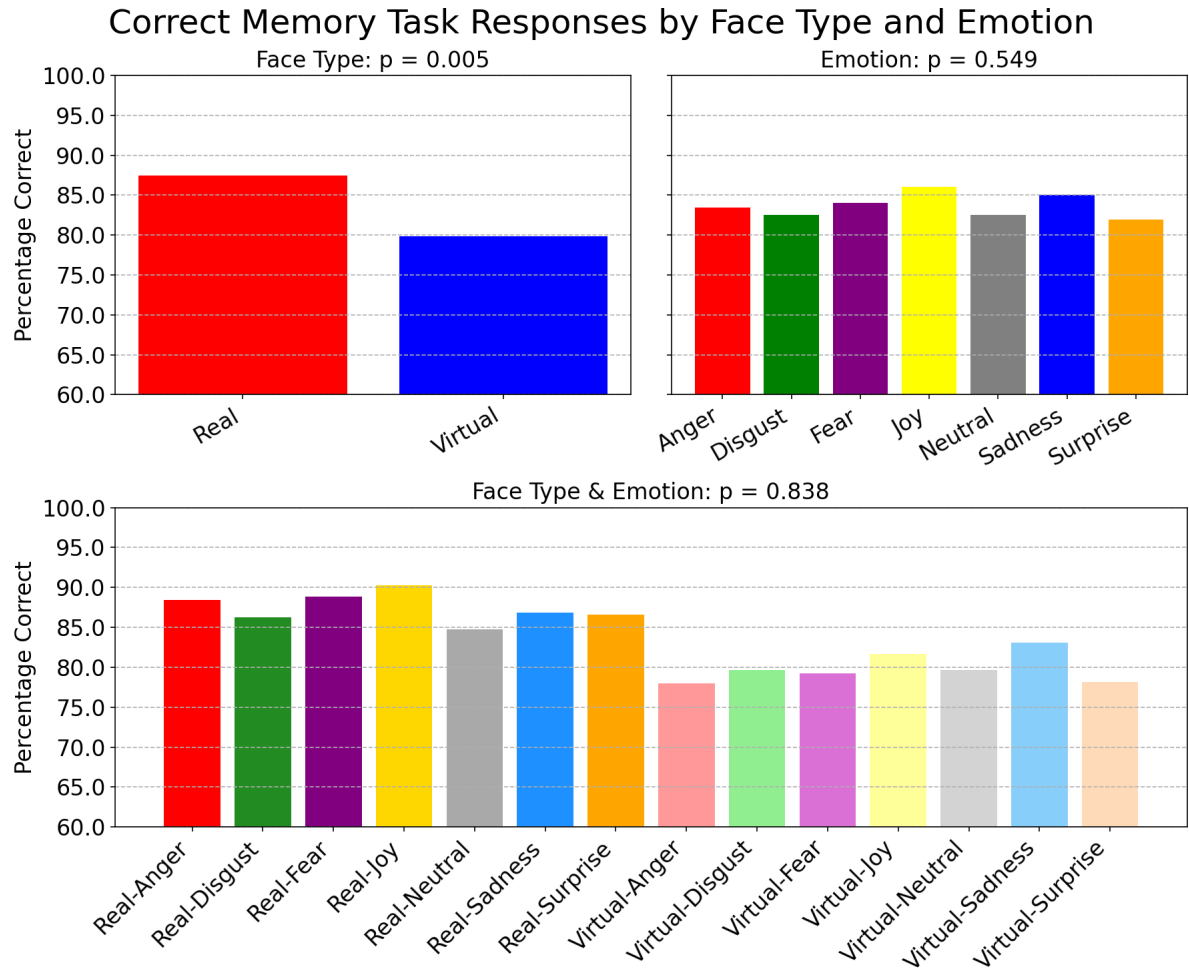


Figure 3.10: Proportion correct by condition in the memory task, plotted separately for real and virtual faces, for each emotion, and the interaction between face type and emotion. The  $p$ -values indicate the significance of the main effects and interaction.

# Chapter 4

## Discussion

With the rise of video games and generative AI technologies, humans are exposed to virtual faces daily. Yet, how our brain process these faces, and their emotions has received little attention. We used functional Near-Infrared Spectroscopy (fNIRS) to capture the brain's hemodynamic response during the processing of real-versus-virtual emotional facial expressions. We used complimentary analytic techniques related to activation magnitude, which captures overall changes in strength of neural response, and functional connectivity mapping, which tracks coherence across brain regions in response to the stimuli. Our goal was to address the following hypotheses: 1) there will be significant differences in activation patterns and functional connectivity profiles when comparing virtual faces to real faces, and 2) different emotional expressions will elicit distinct activation patterns and functional connectivity profiles.

Overall, we found distinct neural mechanisms associated with processing of real-vs-virtual faces, in addition to different emotions on real and virtual faces. That is, the magnitude of the neural response differentiating real and virtual faces, along with the different emotions on the two face types were confined primarily to visual regions. However, we found more widespread differences in the connectivity profiles across the brain in response to face type but also across emotions, with fewer connections in visual ar-

eas, and much stronger connectivity in association areas, such as frontal, parietal and temporal areas. The connectivity analyses also revealed that emotions can be clustered based on the degree of similarity of neural response they evoke. Together these results suggest that real and virtual faces are differentially processed based on visual properties, whereas emotions on real vs virtual faces evoke distinct neural responses distributed across higher-order association areas.

We found the magnitude of neural responses between real and virtual faces were restricted to channels over the occipital region, partially supporting our first hypothesis. This suggests that the brain responds differently to real and virtual faces exclusively in the strength of the neural response in visual areas. Conversely, the functional connectivity analysis revealed distinct neural connectivity patterns associated with processing of real and virtual faces, supporting our first hypothesis, with significantly greater connectivity between the central/temporal, parietal, and left-frontal regions when processing real faces compared to virtual faces. This shows that the broader connectivity changes reflect more complex, distributed processing for real faces compared to virtual ones, indicating that real faces engage higher inter-regional network coordination, a level of processing that virtual faces, despite being recognized as faces, categorically fail to engage. Interestingly, this juxtaposition suggests that while the level of activation in these regions remains stable, the similarity in HbT activity suggests that these regions are prioritized for the processing of real faces over virtual faces.

Our finding that virtual faces elicit greater left occipital activation compared to real faces aligns with evidence that face realism modulates visual processing in a complex manner. The N170 EEG component, reflecting early face perception, is influenced by perceived realism in a u-shaped fashion, while the later Late Positive Potential (LPP) increases continuously with face realism (Schindler et al., 2017). Notably, the N170 generators differ between highly stylized and very realistic faces, suggesting distinct neural processes are engaged depending on realism. The LPP enhancement with increasing

realism is associated with broader occipito-parietal activity, converging with our fNIRS results that show stronger left occipital activation for virtual faces. This indicates that the neural response to virtual faces reflects the perceptual demands of artificial stimuli in the occipital area. Face perception reliably activates the lateral fusiform gyrus, typically bilaterally but most robustly on the right hemisphere (Haxby et al., 2000). This region shows greater responses to faces than to non-face objects. Although fNIRS cannot directly measure deep structures like the fusiform gyrus, our results likely reflect compensatory processing in functionally connected occipital regions that support the fusiform face area when it encounters perceptually challenging stimuli. This compensatory mechanism may manifest as the increased left occipital activation we observed for virtual faces, as these upstream visual areas work harder to provide adequate facial feature extraction to downstream face-processing networks.

Our functional connectivity analysis revealed distinct neural connectivity patterns associated with processing both real and virtual faces, suggesting that the realism of facial stimuli modulates the underlying brain network dynamics during face processing. We observed stronger connectivity when processing real faces across parietal, frontal, and central/temporal regions. Cross-brain coherence in left frontal, temporal, and parietal regions has been observed during social interaction and live eye-to-eye contact (Hirsch et al., 2017). A notable limitation of their study was that there was no occipital coverage, but given that our findings found no significant connectivity differences in the left or right occipital region, this suggests that the occipital region may not be as involved in these processes. These findings further support the notion that real face recognition engages a broader and more coherent neural network. EEG data has revealed statistically significant differences in brain activation between real and synthetic stimuli, with participants correctly identifying real versus synthetic faces with 77% accuracy, suggesting a greater sensitivity to facial authenticity (Tarchi et al., 2023). Together, these results align with our connectivity analysis, reinforcing the notion that real faces engage brain networks,

particularly in emotional and cognitive processing regions, more robustly than synthetic counterparts.

The emotional expressions on real and virtual faces revealed differences in the activation of participants' neural responses, particularly in the occipital, right parietal, and left central/temporal regions. Neutral and surprise expressions elicited more activation than other emotions, suggesting that these expressions are processed differently than the other emotions, possibly due to their ambiguous nature and a greater effort required to interpret them. The functional connectivity analysis showed that there are distinct connectivity patterns associated with processing different emotions, with Fear and Anger eliciting the strongest connectivity, particularly in the left central/temporal cortex across frontal and parietal regions, supporting our second hypothesis. Distinct clusters of emotions emerged from the connectivity analysis, with Fear, Anger, and Joy forming one cluster with stronger connectivity than the other cluster of emotions, which included Disgust, Sadness, Surprise, and Neutral faces. The activation and connectivity analyses show divergent findings, with activation differences primarily in visual regions, while connectivity differences were more widespread across the brain, suggesting that while the initial perception of faces is localized, the emotional processing involves higher-order association areas. We found that across all emotions, visual regions (occipital) showed less connectivity differences, while central/temporal and parietal regions exhibited strong variations, suggesting that the emotional nuances of faces are primarily encoded in these higher-order association areas. This lines up with the constructionist view of emotion, that emotional expressions are decoded in distributed brain networks rather than isolated regions (Barrett, 2006b).

There is consistent evidence of increased brain activation in response to neutral and surprise facial expressions, sometimes even exceeding responses to more overt emotional expressions. Both avatar and human emotional faces activate regions typically involved in emotion processing, such as the bilateral amygdala, fusiform gyri, cerebellum, and

superior temporal gyrus, with neutral face conditions also producing strong amygdala activation, suggesting that the amygdala may not only respond to emotional intensity, but also to the social relevance of faces in general (Moser et al., 2007). This aligns with previous findings showing that some neurons in the temporal lobe and amygdala are tuned to detect faces rather than specific emotions. fMRI studies comparing responses to neutral and scrambled faces have revealed robust activation in regions like the fusiform gyri, amygdalae, entorhinal cortices, and superior temporal sulcus during neutral face viewing (Kesler/West et al., 2001). These findings confirm that emotionally neutral faces still engage core regions involved in face perception and social processing, likely due to their ambiguous or uncertain emotional content. Prior fnIRS and fMRI literature has found inconsistent results for emotional face processing in the PFC, with some studies reporting increases in oxygenated hemoglobin in regions like the medial and ventral PFC, while others showed decreases or no change, depending on the emotion or brain region (Westgarth et al., 2021). These findings and our own challenge the assumption that processing more salient emotions result in greater activation, perhaps the way we process faces has more to do with the connectivity patterns and the networks that are engaged, rather than the magnitude of activation in specific regions.

Fearful faces signal potential threat, and the interpretation of these cues depends on contextual factors, whereas Anger signals the source of threat. Fear processing engages the amygdala, particularly when eye gaze is not directed at the viewer compared to when it is (Cushing et al., 2018). Connectivity from the amygdala to the dorsolateral prefrontal cortex (dlPFC) differs when processing fearful versus sad facial expressions, with increased connectivity when processing fearful faces compared to sad faces, attributing this to the higher salience and arousal associated with fear (Jamieson et al., 2021; Adolphs, 2013). This pattern lines up with our emotion connectivity summary heatmap (Figure 3.7), where fearful faces show robust network engagement relative to others. Additionally, facial emotion expressions can be successfully decoded from functional connec-

tivity patterns, and the networks identified include brain regions beyond the conventional face-selective areas (Liang et al., 2018). This points to Fear as a highly salient emotion that engages a broader network of brain regions, compared to other emotions.

Our count of significantly different channels pairs across all emotions found minimal connectivity differences among left and right occipital ROI, while central/temporal and parietal regions varied strongly, as indicated by the asterisks and carets (Figure 3.8). We found only 20-40 significantly different channels in the occipital regions, compared to 100-120 in the central/temporal and parietal regions, indicating a structural difference in how these regions process emotional faces. This fits with models of face perception, where early visual areas (e.g., occipital face area) feed into higher-level hubs like the fusiform face area. Effective connectivity analyses reveal dynamic modulation between occipital, frontal, and subcortical regions, but early visual areas remain relatively stable across emotion conditions, with emotional discrimination only arising in higher circuits (Underwood et al., 2021). This suggests that while occipital areas are crucial for initial face processing, the emotional nuances of faces are primarily encoded in more distributed networks involving parietal and central/temporal regions, regardless of the emotion presented.

The functional connectivity analysis revealed distinct emotional clusters that reflect underlying similarities in neural processing patterns and arousal characteristics, as seen in Figure 3.7. Anger and Joy also produced notably strong connectivity, clustering with Fear in our summary heatmap, suggesting these emotions share common neural network engagement patterns despite their different valence profiles. This clustering pattern aligns with dimensional models of emotion that emphasize arousal as a key organizing principle, where high-arousal emotions like Fear, Anger, and Joy engage more extensive and coherent neural networks than their low-arousal counterparts (Ke et al., 2025). Lower connectivity for Disgust, Sadness, Surprise, and Neutral faces supports the idea that these emotions have lower arousal or social salience compared to Fear, Anger, and Joy.

The emergence of these two distinct clusters, one characterized by high connectivity (Fear, Anger, Joy) and another by relatively lower connectivity (Disgust, Sadness, Surprise, Neutral), suggests that the brain’s functional architecture organizes emotional face processing along arousal dimensions. This finding is particularly important for understanding how virtual characters and avatars might be designed to maximize/minimize neural engagement, as high-arousal emotional expressions appear to recruit broader brain networks regardless of face realism.

Our findings align with a growing consensus: real faces are remembered more accurately than artificial ones, even though both are processed as faces. Artificial faces are remembered less efficiently and discriminated slightly worse than real faces, supporting the hypothesis that “out-group” faces, those that are less familiar or realistic, are processed differently ([Balas and Pacella, 2015](#)). Complementing this, virtual faces trigger higher false alarm rates, a sign of reduced memory specificity, despite matched visual features and equivalent overall recognition sensitivity ([Kätsyri, 2018](#)). Participants also rated these faces as eerier, highlighting a connection between reduced perceptual expertise and the uncanny valley experience. This suggests that artificial faces engage face-specific processing yet are represented more weakly in memory. Real faces, compared to computer-generated faces, have been associated with poorer performance in an implicit catch trial task, which was interpreted as reflecting an involuntary attentional response toward human faces, which are highly familiar and socially salient visual stimuli ([Kätsyri et al., 2020](#)). The automatic allocation of attention to real faces may have interfered with participants’ ability to withhold a motor response until the catch stimulus appeared, as required by the task. This is consistent with our finding that participants performed better on our memory task for real faces than virtual ones. Enhancing familiarity through exposure ([Park et al., 2021](#)) or increasing realism could help bridge this memory gap. Neuroscientific and evolutionary theories also propose that the human brain includes specialized modules (e.g., the fusiform face area), are highly attuned

to natural facial features ([Burke and Sulikowski, 2013](#)). These modules are refined by experience and optimized for identity recognition, which may not be fully triggered by virtual faces, due to limited exposure or differences in visual features. This may signal evolutionary utility in processing real, familiar faces, and why virtual faces, even when perceived as faces, do not engage the same neural mechanisms as real faces.

## 4.1 Limitations and Future Directions

This study was the first to use fNIRS to examine neural responses to real versus virtual emotional faces, providing novel insights into how face realism and emotion interact in the brain. However, several limitations should be acknowledged. First, since we recruited only from Ontario Tech University's undergraduate student body, our sample of students were limited to that relatively young age range and community, and likely are more educated and technologically savvy than the general population. This may limit the generalizability of our findings to broader populations, particularly older adults or those with less exposure to virtual characters/avatars. As well, many participants did not pass our signal quality checks, due to reasons such as hair color/texture affecting the signal quality ([Holmes et al., 2024](#)). Additionally, our sample was predominantly female, which may have influenced our results as females and males may differ in their accuracy and sensitivity when categorizing facial emotions; for example, females have been shown to outperform males in identifying fearful faces ([Weisenbach et al., 2014](#)). Men have also been found to have a differential neural response depending upon the emotion presented ([Kesler/West et al., 2001](#)). Future studies should include a wider range of participants, ideally representing the general population.

Second, since the virtual faces used in this study were all from one dataset (UIB-VFED), they were all of similar realism and stylization. Since neural responses to virtual faces vary with realism, our findings may not generalize to other virtual face datasets

with different levels of realism or stylization (Schindler et al., 2017). Future work should explore a wider range of virtual face styles and realism levels to better understand how these factors influence neural processing.

## 4.2 Conclusion

The present study investigated how the human brain processes emotional expressions on real versus virtual faces, using functional near-infrared spectroscopy (fNIRS) to assess both activation magnitude and functional connectivity. By directly comparing hemodynamic responses to real and virtual faces across a range of basic emotions, we aimed to determine whether face realism modulates neural responses, and whether these effects extend beyond local activation to distributed network interactions. We found that virtual faces elicited greater activation in the left occipital region, suggesting increased perceptual demands, while real faces were associated with stronger distributed connectivity and better recall performance in a memory task. Neutral and surprise expressions evoked the strongest activation, whereas fear and anger engaged broader neural networks. These findings highlight the complex interplay between face realism and emotion processing, suggesting that while virtual faces are perceived as faces, they do not recruit the same neural mechanisms as real ones. Emotional expressions appear to be decoded in distributed brain networks rather than isolated regions. These results offer novel insights into the neural mechanisms of emotional face perception in the context of increasingly prevalent virtual social interactions. Future research should examine how varying levels of virtual face realism and stylization influence neural responses and social cognition.

# Bibliography

- Adolphs, R. (2013). The Biology of Fear. *Current Biology*, 23(2):R79–R93. Publisher: Elsevier.
- Aviezer, H., Bentin, S., Dudarev, V., and Hassin, R. R. (2011). The automaticity of emotional face-context integration. *Emotion (Washington, D.C.)*, 11(6):1406–1414.
- Balas, B. and Pacella, J. (2015). Artificial faces are harder to remember. *Computers in human behavior*, 52:331–337.
- Barrett, L. F. (2006a). Are Emotions Natural Kinds? *Perspectives on Psychological Science*, 1(1):28–58.
- Barrett, L. F. (2006b). Solving the emotion paradox: Categorization and the experience of emotion. *Personality and Social Psychology Review*, 10(1):20–46. PMID: 16430327.
- Bastos, A. M. and Schoffelen, J.-M. (2016). A Tutorial Review of Functional Connectivity Analysis Methods and Their Interpretational Pitfalls. *Frontiers in Systems Neuroscience*, 9. Publisher: Frontiers.
- Bendall, R. C. A., Eachus, P., and Thompson, C. (2016). A Brief Review of Research Using Near-Infrared Spectroscopy to Measure Activation of the Prefrontal Cortex during Emotional Processing: The Importance of Experimental Design. *Frontiers in Human Neuroscience*, 10. Publisher: Frontiers.

- Bergmann, T., Froese, L., Gomez, A., Sainbhi, A. S., Vakitbilir, N., Islam, A., Stein, K., Marquez, I., Amenta, F., Park, K., Ibrahim, Y., and Zeiler, F. A. (2023). Evaluation of Morlet Wavelet Analysis for Artifact Detection in Low-Frequency Commercial Near-Infrared Spectroscopy Systems. *Bioengineering*, 11(1):0.
- Brooks, J. A. and Freeman, J. B. (2018). Conceptual knowledge predicts the representational structure of facial emotion perception. *Nature human behaviour*, 2(8):581–591.
- Bulgarelli, C., Blasi, A., McCann, S., Milosavljevic, B., Ghillia, G., Mbye, E., Touray, E., Fadera, T., Acolatse, L., Moore, S. E., Lloyd-Fox, S., Elwell, C. E., Eggebrecht, A. T., and Team, t. B. S. (2025). Growth in early infancy drives optimal brain functional connectivity which predicts cognitive flexibility in later childhood. Pages: 2024.01.02.573930 Section: New Results.
- Burke, D. and Sulikowski, D. (2013). The Evolution of Holistic Processing of Faces. *Frontiers in Psychology*, 4:11.
- Calbi, M., Heimann, K., Barratt, D., Siri, F., Umiltà, M. A., and Gallese, V. (2017). How Context Influences Our Perception of Emotional Faces: A Behavioral Study on the Kuleshov Effect. *Frontiers in Psychology*, 8. Publisher: Frontiers.
- Chen, Y., Stephani, T., Bagdasarian, M. T., Hilsmann, A., Eisert, P., Villringer, A., Bosse, S., Gaebler, M., and Nikulin, V. V. (2024). Realness of face images can be decoded from non-linear modulation of EEG responses. *Scientific Reports*, 14(1):5683. Publisher: Nature Publishing Group.
- Conley, M. I., Dellarco, D. V., Rubien-Thomas, E., Cohen, A. O., Cervera, A., Tottenham, N., and Casey, B. (2018). The racially diverse affective expression (RADIATE) face stimulus set. *Psychiatry Research*, 270:1059–1067.
- Cowen, A. S., Keltner, D., Schroff, F., Jou, B., Adam, H., and Prasad, G. (2021). Sixteen

- facial expressions occur in similar contexts worldwide. *Nature*, 589(7841):251–257. Publisher: Nature Publishing Group.
- Cui, X., Bray, S., and Reiss, A. L. (2010). Functional near infrared spectroscopy (NIRS) signal improvement based on negative correlation between oxygenated and deoxygenated hemoglobin dynamics. *NeuroImage*, 49(4):3039–3046.
- Cushing, C. A., Im, H. Y., Adams, R. B., Ward, N., Albohn, D. N., Steiner, T. G., and Kveraga, K. (2018). Neurodynamics and connectivity during facial fear perception: The role of threat exposure and signal congruity. *Scientific Reports*, 8(1):2776. Publisher: Nature Publishing Group.
- De Borst, A. W. and De Gelder, B. (2015). Is it the real deal? Perception of virtual characters versus humans: an affective cognitive neuroscience perspective. *Frontiers in Psychology*, 6.
- Dyck, M., Winbeck, M., Leiberg, S., Chen, Y., Gur, R. C., and Mathiak, K. (2008). Recognition Profile of Emotions in Natural and Virtual Faces. *PLOS ONE*, 3(11):e3628. Publisher: Public Library of Science.
- Ekman, P. and Friesen, W. V. (1971). Constants across cultures in the face and emotion. *Journal of personality and social psychology*, 17(2):124.
- Ekman, P. and Friesen, W. V. (1978). Facial action coding system. *Environmental Psychology & Nonverbal Behavior*.
- Faita, C., Vanni, F., Lorenzini, C., Carrozzino, M., Tanca, C., and Bergamasco, M. (2015). Perception of Basic Emotions from Facial Expressions of Dynamic Virtual Avatars. In De Paolis, L. T. and Mongelli, A., editors, *Augmented and Virtual Reality*, volume 9254, pages 409–419. Springer International Publishing, Cham. Series Title: Lecture Notes in Computer Science.

- Fishburn, F. A., Ludlum, R. S., Vaidya, C. J., and Medvedev, A. V. (2019). Temporal Derivative Distribution Repair (TDDR): A motion correction method for fNIRS. *NeuroImage*, 184:171–179.
- Friston, K. J. (2007). *Statistical parametric mapping: the analysis of functional brain images*. Elsevier / Academic Press, Amsterdam Boston, 1st ed edition.
- García, A. S., Fernández-Sotos, P., Vicente-Querol, M. A., Lahera, G., Rodriguez-Jimenez, R., and Fernández-Caballero, A. (2020). Design of reliable virtual human facial expressions and validation by healthy people. *Integrated Computer-Aided Engineering*, 27(3):287–299.
- Gramfort, A., Luessi, M., Larson, E., Engemann, D. A., Strohmeier, D., Brodbeck, C., Goj, R., Jas, M., Brooks, T., Parkkonen, L., and Hämäläinen, M. (2013). MEG and EEG data analysis with MNE-Python. *Frontiers in Neuroscience*, 7. Publisher: Frontiers.
- Hakim, U., De Felice, S., Pinti, P., Zhang, X., Noah, J., Ono, Y., Burgess, P. W., Hamilton, A., Hirsch, J., and Tachtsidis, I. (2023). Quantification of inter-brain coupling: A review of current methods used in haemodynamic and electrophysiological hyperscanning studies. *NeuroImage*, 280:120354.
- Haxby, J. V., Hoffman, E. A., Gobbini, M. I., Haxby, J. V., Hoffman, E. A., Gobbini, M. I., Haxby, J. V., Hoffman, E. A., and Gobbini, M. I. (2000). The distributed human neural system for face perception. *Trends in Cognitive Sciences*, 4(6):223–233. Publisher: Elsevier.
- Hernandez, S. M. and Pollonini, L. (2020). NIRSpot: A Tool for Quality Assessment of fNIRS Scans. In *Biophotonics Congress: Biomedical Optics 2020 (Translational, Microscopy, OCT, OTS, BRAIN)*, page BM2C.5, Washington, DC. Optica Publishing Group.

- Hirsch, J., Zhang, X., Noah, J. A., and Ono, Y. (2017). Frontal temporal and parietal systems synchronize within and across brains during live eye-to-eye contact. *NeuroImage*, 157:314–330.
- Hocke, L. M., Oni, I. K., Duszynski, C. C., Corrigan, A. V., Frederick, B. D., and Dunn, J. F. (2018). Automated Processing of fNIRS Data—A Visual Guide to the Pitfalls and Consequences. *Algorithms*, 11(5):67. Number: 5 Publisher: Multidisciplinary Digital Publishing Institute.
- Holmes, M., Aalto, D., and Cummine, J. (2024). Opening the dialogue: A preliminary exploration of hair color, hair cleanliness, light, and motion effects on fNIRS signal quality. *PLOS ONE*, 19(5):e0304356. Publisher: Public Library of Science.
- Hortensius, R., Hekele, F., and Cross, E. S. (2018). The Perception of Emotion in Artificial Agents. *IEEE Transactions on Cognitive and Developmental Systems*, 10(4):852–864.
- Hu, P., Wang, P., Zhao, R., Yang, H., and Biswal, B. B. (2023). Characterizing the spatiotemporal features of functional connectivity across the white matter and gray matter during the naturalistic condition. *Frontiers in Neuroscience*, 17. Publisher: Frontiers.
- Huppert, T. J. (2016). Commentary on the statistical properties of noise and its implication on general linear models in functional near-infrared spectroscopy. *Neurophotonics*, 3(1):010401. Publisher: SPIE.
- Jack, R. E., Garrod, O. G. B., Yu, H., Caldara, R., and Schyns, P. G. (2012). Facial expressions of emotion are not culturally universal. *Proceedings of the National Academy of Sciences*, 109(19):7241–7244. Publisher: Proceedings of the National Academy of Sciences.

- Jamieson, A. J., Davey, C. G., and Harrison, B. J. (2021). Differential Modulation of Effective Connectivity in the Brain's Extended Face Processing System by Fearful and Sad Facial Expressions. *eNeuro*, 8(2). Publisher: Society for Neuroscience Section: Research Article: New Research.
- Johnson, M. H., Dziurawiec, S., Ellis, H., and Morton, J. (1991). Newborns' preferential tracking of face-like stimuli and its subsequent decline. *Cognition*, 40(1-2):1–19.
- Ke, J., Song, H., Bai, Z., Rosenberg, M. D., and Leong, Y. C. (2025). Dynamic brain connectivity predicts emotional arousal during naturalistic movie-watching. *PLOS Computational Biology*, 21(4):e1012994. Publisher: Public Library of Science.
- Kegel, L. C., Brugger, P., Frühholz, S., Grunwald, T., Hilfiker, P., Kohnen, O., Loertscher, M. L., Mersch, D., Rey, A., Sollfrank, T., Steiger, B. K., Sternagel, J., Weber, M., and Jokeit, H. (2020). Dynamic human and avatar facial expressions elicit differential brain responses. *Social Cognitive and Affective Neuroscience*, 15(3):303–317.
- Kesler/West, M. L., Andersen, A. H., Smith, C. D., Avison, M. J., Davis, C. E., Kryscio, R. J., and Blonder, L. X. (2001). Neural substrates of facial emotion processing using fMRI. *Cognitive Brain Research*, 11(2):213–226.
- Kinder, K. T., Heim, H. L. R., Parker, J., Lowery, K., McCraw, A., Eddings, R. N., Defenderfer, J., Sullivan, J., and Buss, A. T. (2022). Systematic review of fNIRS studies reveals inconsistent chromophore data reporting practices. *Neurophotonics*, 9(4):040601.
- Kocsis, L., Herman, P., and Eke, A. (2006). The modified Beer–Lambert law revisited. *Physics in Medicine & Biology*, 51(5):N91.
- Kragel, P. A. and LaBar, K. S. (2016). Decoding the Nature of Emotion in the Brain. *Trends in cognitive sciences*, 20(6):444–455.

- Kätsyri, J. (2018). Those Virtual People all Look the Same to me: Computer-Rendered Faces Elicit a Higher False Alarm Rate Than Real Human Faces in a Recognition Memory Task. *Frontiers in Psychology*, 9:1362.
- Kätsyri, J., de Gelder, B., and de Borst, A. W. (2020). Amygdala responds to direct gaze in real but not in computer-generated faces. *NeuroImage*, 204:116216.
- Kätsyri, J., Mäkäräinen, M., and Takala, T. (2017). Testing the ‘uncanny valley’ hypothesis in semirealistic computer-animated film characters: An empirical evaluation of natural film stimuli. *International Journal of Human-Computer Studies*, 97:149–161.
- Lee, T.-H., Choi, J.-S., and Cho, Y. S. (2012). Context modulation of facial emotion perception differed by individual difference. *PloS One*, 7(3):e32987.
- Liang, Y., Liu, B., Li, X., and Wang, P. (2018). Multivariate Pattern Classification of Facial Expressions Based on Large-Scale Functional Connectivity. *Frontiers in Human Neuroscience*, 12. Publisher: Frontiers.
- Lindquist, K. A., Wager, T. D., Kober, H., Bliss-Moreau, E., and Barrett, L. F. (2012). The brain basis of emotion: A meta-analytic review. *Behavioral and Brain Sciences*, 35(3):121–143.
- Luke, R., Larson, E. D., Shader, M. J., Innes-Brown, H., Yper, L. V., Lee, A. K. C., Sowman, P. F., and McAlpine, D. (2021). Analysis methods for measuring passive auditory fNIRS responses generated by a block-design paradigm. *Neurophotonics*, 8(2):025008. Publisher: SPIE.
- Matsumoto, D. and Wilson, M. (2022). A half-century assessment of the study of culture and emotion. *Journal of Cross-Cultural Psychology*, 53(7-8):917–934.
- Miranda de Sá, A. M. F. L., Ferreira, D. D., Dias, E. W., Mendes, E. M. A. M., and Felix, L. B. (2009). Coherence estimate between a random and a periodic signal: Bias,

- variance, analytical critical values, and normalizing transforms. *Journal of the Franklin Institute*, 346(9):841–853.
- Mori, M., MacDorman, K. F., and Kageki, N. (2012). The Uncanny Valley [From the Field]. *IEEE Robotics & Automation Magazine*, 19(2):98–100.
- Moser, E., Derntl, B., Robinson, S., Fink, B., Gur, R. C., and Grammer, K. (2007). Amygdala activation at 3T in response to human and avatar facial expressions of emotions. *Journal of Neuroscience Methods*, 161(1):126–133.
- Oliver, M. M. and Amengual Alcover, E. (2020). UIBVFED: Virtual facial expression dataset. *PLOS ONE*, 15(4):e0231266.
- Palmer, C. J. and Clifford, C. W. G. (2020). Face Pareidolia Recruits Mechanisms for Detecting Human Social Attention. *Psychological Science*, 31(8):1001–1012. Publisher: SAGE Publications Inc.
- Park, S., Kim, S. P., and Whang, M. (2021). Individual's Social Perception of Virtual Avatars Embodied with Their Habitual Facial Expressions and Facial Appearance. *Sensors*, 21(17):5986.
- Peirce, J., Gray, J. R., Simpson, S., MacAskill, M., Höchenberger, R., Sogo, H., Kastman, E., and Lindeløv, J. K. (2019). PsychoPy2: Experiments in behavior made easy. *Behavior Research Methods*, 51(1):195–203.
- Pinti, P., Scholkmann, F., Hamilton, A., Burgess, P., and Tachtsidis, I. (2019). Current Status and Issues Regarding Pre-processing of fNIRS Neuroimaging Data: An Investigation of Diverse Signal Filtering Methods Within a General Linear Model Framework. *Frontiers in Human Neuroscience*, 12.
- Pollonini, L., Bortfeld, H., and Oghalai, J. S. (2016). PHOEBC: a method for real time

- mapping of optodes-scalp coupling in functional near-infrared spectroscopy. *Biomedical Optics Express*, 7(12):5104–5119. Publisher: Optica Publishing Group.
- Powell, L. J., Kosakowski, H. L., and Saxe, R. (2018). Social Origins of Cortical Face Areas. *Trends in cognitive sciences*, 22(9):752–763.
- Reddy, P., Izzetoglu, M., Shewokis, P. A., Sangobowale, M., Diaz-Arrastia, R., and Izzetoglu, K. (2021). Evaluation of fNIRS signal components elicited by cognitive and hypercapnic stimuli. *Scientific Reports*, 11(1):23457. Publisher: Nature Publishing Group.
- Ruttkay, Z. (2009). Cultural dialects of real and synthetic emotional facial expressions. *AI & SOCIETY*, 24(3):307–315.
- Sato, W., Yoshikawa, S., Kochiyama, T., and Matsumura, M. (2004). The amygdala processes the emotional significance of facial expressions: an fMRI investigation using the interaction between expression and face direction. *NeuroImage*, 22(2):1006–1013.
- Schindler, S., Zell, E., Botsch, M., and Kissler, J. (2017). Differential effects of face-realism and emotion on event-related brain potentials and their implications for the uncanny valley theory. *Scientific Reports*, 7(1):45003. Publisher: Nature Publishing Group.
- Schneider, S., Christensen, A., Häußinger, F. B., Fallgatter, A. J., Giese, M. A., and Ehlis, A.-C. (2014). Show me how you walk and i tell you how you feel — a functional near-infrared spectroscopy study on emotion perception based on human gait. *NeuroImage*, 85:380–390. Celebrating 20 Years of Functional Near Infrared Spectroscopy (fNIRS).
- Scholkmann, F., Metz, A. J., and Wolf, M. (2014). Measuring tissue hemodynamics and oxygenation by continuous-wave functional near-infrared spectroscopy—how robust are the different calculation methods against movement artifacts? *Physiological Measurement*, 35(4):717. Publisher: IOP Publishing.

- Seabold, S. and Perktold, J. (2010). statsmodels: Econometric and statistical modeling with python. In *9th Python in Science Conference*.
- Sheehan, M. J. and Nachman, M. W. (2014). Morphological and population genomic evidence that human faces have evolved to signal individual identity. *Nature Communications*, 5(1):4800. Publisher: Nature Publishing Group.
- Singh, A. K. and Dan, I. (2006). Exploring the false discovery rate in multichannel NIRS. *NeuroImage*, 33(2):542–549.
- Sollfrank, T., Kohnen, O., Hilfiker, P., Kegel, L. C., Jokeit, H., Brugger, P., Loertscher, M. L., Rey, A., Mersch, D., Sternagel, J., Weber, M., and Grunwald, T. (2021). The Effects of Dynamic and Static Emotional Facial Expressions of Humans and Their Avatars on the EEG: An ERP and ERD/ERS Study. *Frontiers in Neuroscience*, 15. Publisher: Frontiers.
- Tachtsidis, I. and Scholkmann, F. (2016). False positives and false negatives in functional near-infrared spectroscopy: issues, challenges, and the way forward. *Neurophotonics*, 3(3):031405. Publisher: SPIE.
- Tak, S. and Ye, J. C. (2014). Statistical analysis of fNIRS data: A comprehensive review. *NeuroImage*, 85:72–91.
- Tarchi, P., Calà, F., Frassineti, L., and Lanatà, A. (2023). Electroencephalographic Correlates in Synthetic and Real Emotional Face Stimulation. In *2023 45th Annual International Conference of the IEEE Engineering in Medicine & Biology Society (EMBC)*, pages 1–4. ISSN: 2694-0604.
- Underwood, R., Tolmeijer, E., Wibroe, J., Peters, E., and Mason, L. (2021). Networks underpinning emotion: A systematic review and synthesis of functional and effective connectivity. *Neuroimage*, 243:118486.

- Weisenbach, S. L., Rapport, L. J., Briceno, E. M., Haase, B. D., Vederman, A. C., Bieliauskas, L. A., Welsh, R. C., Starkman, M. N., McInnis, M. G., Zubieta, J.-K., and Langenecker, S. A. (2014). Reduced emotion processing efficiency in healthy males relative to females. *Social Cognitive and Affective Neuroscience*, 9(3):316–325.
- Westgarth, M. M. P., Hogan, C. A., Neumann, D. L., and Shum, D. H. K. (2021). A systematic review of studies that used NIRS to measure neural activation during emotion processing in healthy individuals. *Social Cognitive and Affective Neuroscience*, 16(4):345–369.
- Willis, J. and Todorov, A. (2006). First impressions: Making up your mind after a 100-ms exposure to a face. *Psychological Science*, 17(7):592–598. PMID: 16866745.
- Xu, G., Zhang, M., Wang, Y., Liu, Z., Huo, C., Li, Z., and Huo, M. (2017). Functional connectivity analysis of distracted drivers based on the wavelet phase coherence of functional near-infrared spectroscopy signals. *PLOS ONE*, 12(11):e0188329. Publisher: Public Library of Science.
- Yücel, M. A., Selb, J. J., Huppert, T. J., Franceschini, M. A., and Boas, D. A. (2017). Functional Near Infrared Spectroscopy: Enabling routine functional brain imaging. *Current Opinion in Biomedical Engineering*, 4:78–86.

# Data Availability

The data generated during this study has been made openly available at the Open Science Framework (OSF) [here](#).

# Appendix A

## GLM Contrasts

Table A.1: Table of significant contrast results from the GLM analysis.

| Contrast           | Region              | Ch Name     | Coef.  | Std.Err. | <i>z</i> | <i>p<sub>fdr</sub></i> |
|--------------------|---------------------|-------------|--------|----------|----------|------------------------|
| Real - Virtual     | L. Occipital        | S23 D15 hbt | -1.550 | 0.394    | -3.937   | 0.009                  |
| Joy - Neutral      | R. Parietal         | S20 D29 hbt | 2.611  | 0.623    | 4.194    | 0.001                  |
| Joy - Neutral      | R. Occipital        | S23 D30 hbt | -3.144 | 0.623    | -5.050   | 0.000                  |
| Joy - Surprise     | R. Occipital        | S23 D16 hbt | -2.884 | 0.647    | -4.460   | 0.001                  |
| Joy - Surprise     | L. Central/Temporal | S25 D6 hbt  | -2.379 | 0.647    | -3.679   | 0.012                  |
| Fear - Neutral     | R. Occipital        | S23 D30 hbt | -2.126 | 0.557    | -3.819   | 0.014                  |
| Fear - Surprise    | R. Parietal         | S20 D29 hbt | -2.048 | 0.568    | -3.606   | 0.032                  |
| Anger - Neutral    | R. Occipital        | S23 D30 hbt | -3.620 | 0.652    | -5.547   | 0.000                  |
| Disgust - Surprise | R. Occipital        | S23 D16 hbt | -2.507 | 0.640    | -3.920   | 0.005                  |
| Disgust - Surprise | L. Central/Temporal | S25 D6 hbt  | -2.531 | 0.640    | -3.958   | 0.005                  |
| Sadness - Neutral  | L. Frontal          | S4 D6 hbt   | -2.257 | 0.601    | -3.754   | 0.018                  |
| Sadness - Surprise | L. Frontal          | S4 D6 hbt   | -2.610 | 0.673    | -3.879   | 0.011                  |
| Sadness - Surprise | R. Parietal         | S20 D29 hbt | -2.304 | 0.673    | -3.425   | 0.032                  |

Continued on next page

Table A.1: Table of significant contrast results from the GLM analysis.

| Contrast                    | Region              | Ch Name     | Coef.  | Std.Err. | <i>z</i> | <i>p</i> <sub>fdr</sub> |
|-----------------------------|---------------------|-------------|--------|----------|----------|-------------------------|
| Neutral - Surprise          | R. Parietal         | S20 D29 hbt | -2.653 | 0.625    | -4.247   | 0.002                   |
| Neutral - Surprise          | R. Occipital        | S23 D30 hbt | 2.461  | 0.625    | 3.940    | 0.004                   |
| Real Joy - Real Disgust     | R. Occipital        | S23 D30 hbt | -5.344 | 1.093    | -4.889   | 0.000                   |
| Real Joy - Real Sadness     | R. Occipital        | S24 D30 hbt | -3.816 | 0.964    | -3.958   | 0.008                   |
| Real Joy - Real Neutral     | R. Occipital        | S23 D30 hbt | -5.786 | 0.980    | -5.906   | 0.000                   |
| Real Joy - Real Surprise    | R. Frontal          | S9 D19 hbt  | 3.093  | 0.997    | 3.101    | 0.050                   |
| Real Joy - Real Surprise    | L. Occipital        | S23 D15 hbt | -3.754 | 0.997    | -3.764   | 0.017                   |
| Real Joy - Real Surprise    | R. Occipital        | S23 D16 hbt | -3.577 | 0.997    | -3.587   | 0.017                   |
| Real Joy - Real Surprise    | L. Central/Temporal | S25 D6 hbt  | -3.293 | 0.997    | -3.302   | 0.033                   |
| Real Joy - Virtual Joy      | L. Occipital        | S32 D15 hbt | 3.484  | 0.966    | 3.607    | 0.032                   |
| Real Joy - Virtual Fear     | L. Occipital        | S23 D15 hbt | -3.384 | 0.965    | -3.506   | 0.023                   |
| Real Joy - Virtual Fear     | R. Occipital        | S23 D30 hbt | -3.649 | 0.965    | -3.781   | 0.016                   |
| Real Joy - Virtual Disgust  | L. Occipital        | S23 D15 hbt | -4.428 | 0.986    | -4.490   | 0.001                   |
| Real Joy - Virtual Sadness  | L. Occipital        | S23 D15 hbt | -4.435 | 0.973    | -4.556   | 0.001                   |
| Real Joy - Virtual Surprise | R. Occipital        | S23 D16 hbt | -3.197 | 0.949    | -3.368   | 0.039                   |
| Real Joy - Virtual Surprise | R. Occipital        | S23 D30 hbt | -3.410 | 0.949    | -3.593   | 0.034                   |
| Real Fear - Real Disgust    | R. Occipital        | S23 D30 hbt | -4.918 | 1.087    | -4.522   | 0.001                   |
| Real Fear - Real Neutral    | R. Occipital        | S23 D30 hbt | -5.360 | 0.980    | -5.470   | 0.000                   |
| Real Fear - Virtual Joy     | L. Central/Temporal | S25 D6 hbt  | 4.150  | 1.054    | 3.938    | 0.008                   |
| Real Fear - Virtual Disgust | L. Occipital        | S23 D15 hbt | -4.112 | 1.009    | -4.073   | 0.002                   |
| Real Fear - Virtual Disgust | L. Central/Temporal | S25 D6 hbt  | 4.183  | 1.009    | 4.144    | 0.002                   |
| Real Fear - Virtual Sadness | L. Occipital        | S23 D15 hbt | -4.119 | 1.003    | -4.109   | 0.004                   |
| Real Fear - Virtual Sadness | L. Central/Temporal | S25 D6 hbt  | 3.595  | 1.003    | 3.585    | 0.017                   |

Continued on next page

Table A.1: Table of significant contrast results from the GLM analysis.

| Contrast                       | Region       | Ch Name     | Coef.  | Std.Err. | <i>z</i> | <i>p</i> <sub>fdr</sub> |
|--------------------------------|--------------|-------------|--------|----------|----------|-------------------------|
| Real Anger - Real Disgust      | R. Occipital | S23 D30 hbt | -4.697 | 1.117    | -4.205   | 0.003                   |
| Real Anger - Real Neutral      | R. Occipital | S23 D30 hbt | -5.139 | 0.983    | -5.226   | 0.000                   |
| Real Disgust - Real Surprise   | L. Frontal   | S4 D6 hbt   | -3.742 | 1.107    | -3.380   | 0.025                   |
| Real Disgust - Real Surprise   | L. Occipital | S23 D15 hbt | -4.679 | 1.107    | -4.226   | 0.002                   |
| Real Disgust - Real Surprise   | R. Occipital | S23 D30 hbt | 4.221  | 1.107    | 3.813    | 0.007                   |
| Real Disgust - Virtual Fear    | L. Occipital | S23 D15 hbt | -4.309 | 1.013    | -4.252   | 0.002                   |
| Real Disgust - Virtual Disgust | L. Occipital | S23 D15 hbt | -5.353 | 1.163    | -4.603   | 0.000                   |
| Real Disgust - Virtual Disgust | R. Occipital | S23 D30 hbt | 5.028  | 1.163    | 4.323    | 0.001                   |
| Real Disgust - Virtual Sadness | L. Occipital | S23 D15 hbt | -5.360 | 1.163    | -4.608   | 0.000                   |
| Real Disgust - Virtual Sadness | R. Occipital | S23 D30 hbt | 4.254  | 1.163    | 3.657    | 0.013                   |
| Real Disgust - Virtual Neutral | R. Occipital | S23 D30 hbt | 3.878  | 1.102    | 3.520    | 0.044                   |
| Real Sadness - Real Neutral    | R. Occipital | S23 D30 hbt | -3.749 | 0.912    | -4.110   | 0.002                   |
| Real Sadness - Real Neutral    | R. Occipital | S24 D30 hbt | 4.012  | 0.912    | 4.398    | 0.001                   |
| Real Sadness - Real Surprise   | L. Frontal   | S4 D6 hbt   | -3.743 | 1.059    | -3.534   | 0.021                   |
| Real Sadness - Real Surprise   | R. Occipital | S24 D30 hbt | 4.688  | 1.059    | 4.426    | 0.001                   |
| Real Sadness - Virtual Joy     | R. Occipital | S24 D30 hbt | 3.811  | 1.048    | 3.638    | 0.028                   |
| Real Sadness - Virtual Disgust | L. Occipital | S23 D15 hbt | -3.951 | 1.088    | -3.633   | 0.029                   |
| Real Sadness - Virtual Sadness | L. Occipital | S23 D15 hbt | -3.959 | 1.051    | -3.766   | 0.017                   |
| Real Neutral - Real Surprise   | R. Parietal  | S20 D29 hbt | -3.553 | 0.933    | -3.809   | 0.007                   |
| Real Neutral - Real Surprise   | R. Occipital | S23 D30 hbt | 4.663  | 0.933    | 4.999    | 0.000                   |
| Real Neutral - Virtual Joy     | R. Occipital | S23 D30 hbt | 3.563  | 0.924    | 3.856    | 0.012                   |
| Real Neutral - Virtual Anger   | L. Frontal   | S4 D6 hbt   | 4.371  | 1.009    | 4.330    | 0.002                   |
| Real Neutral - Virtual Anger   | R. Occipital | S23 D30 hbt | 3.737  | 1.009    | 3.702    | 0.011                   |

Continued on next page

Table A.1: Table of significant contrast results from the GLM analysis.

| Contrast                        | Region              | Ch Name     | Coef.  | Std.Err. | <i>z</i> | <i>p</i> <sub>fdr</sub> |
|---------------------------------|---------------------|-------------|--------|----------|----------|-------------------------|
| Real Neutral - Virtual Disgust  | R. Occipital        | S23 D30 hbt | 5.470  | 1.020    | 5.365    | 0.000                   |
| Real Neutral - Virtual Sadness  | L. Frontal          | S4 D6 hbt   | 4.863  | 0.963    | 5.051    | 0.000                   |
| Real Neutral - Virtual Sadness  | R. Occipital        | S23 D30 hbt | 4.696  | 0.963    | 4.877    | 0.000                   |
| Real Neutral - Virtual Neutral  | R. Occipital        | S23 D30 hbt | 4.320  | 0.994    | 4.346    | 0.001                   |
| Real Surprise - Virtual Joy     | L. Frontal          | S4 D6 hbt   | 3.580  | 1.038    | 3.448    | 0.029                   |
| Real Surprise - Virtual Joy     | L. Central/Temporal | S25 D6 hbt  | 4.185  | 1.038    | 4.030    | 0.006                   |
| Real Surprise - Virtual Anger   | L. Frontal          | S4 D6 hbt   | 5.443  | 1.096    | 4.966    | 0.000                   |
| Real Surprise - Virtual Anger   | R. Frontal          | S10 D17 hbt | -3.659 | 1.096    | -3.338   | 0.029                   |
| Real Surprise - Virtual Anger   | L. Occipital        | S23 D15 hbt | 3.907  | 1.096    | 3.565    | 0.019                   |
| Real Surprise - Virtual Disgust | L. Central/Temporal | S25 D6 hbt  | 4.218  | 1.042    | 4.048    | 0.005                   |
| Real Surprise - Virtual Sadness | L. Frontal          | S4 D6 hbt   | 5.935  | 1.000    | 5.937    | 0.000                   |
| Real Surprise - Virtual Sadness | L. Central/Temporal | S7 D6 hbt   | 3.660  | 1.000    | 3.661    | 0.007                   |
| Real Surprise - Virtual Sadness | R. Parietal         | S20 D29 hbt | 4.101  | 1.000    | 4.102    | 0.002                   |
| Real Surprise - Virtual Sadness | L. Central/Temporal | S25 D6 hbt  | 3.630  | 1.000    | 3.631    | 0.007                   |
| Real Surprise - Virtual Neutral | L. Frontal          | S4 D6 hbt   | 3.189  | 1.025    | 3.111    | 0.048                   |
| Real Surprise - Virtual Neutral | R. Frontal          | S9 D19 hbt  | -3.357 | 1.025    | -3.275   | 0.048                   |
| Real Surprise - Virtual Neutral | R. Parietal         | S20 D29 hbt | 3.539  | 1.025    | 3.453    | 0.048                   |
| Real Surprise - Virtual Neutral | L. Occipital        | S31 D15 hbt | -3.254 | 1.025    | -3.174   | 0.048                   |
| Virtual Joy - Virtual Disgust   | L. Occipital        | S32 D15 hbt | -4.343 | 1.008    | -4.308   | 0.002                   |
| Virtual Fear - Virtual Disgust  | R. Occipital        | S23 D30 hbt | 3.333  | 0.928    | 3.590    | 0.034                   |
| Virtual Fear - Virtual Sadness  | L. Frontal          | S4 D6 hbt   | 3.597  | 1.021    | 3.522    | 0.044                   |
| Virtual Anger - Virtual Disgust | L. Frontal          | S4 D6 hbt   | -3.633 | 1.033    | -3.518   | 0.019                   |
| Virtual Anger - Virtual Disgust | L. Occipital        | S23 D15 hbt | -4.581 | 1.033    | -4.436   | 0.001                   |

Continued on next page

Table A.1: Table of significant contrast results from the GLM analysis.

| Contrast                           | Region              | Ch Name     | Coef.  | Std.Err. | <i>z</i> | <i>p<sub>fdr</sub></i> |
|------------------------------------|---------------------|-------------|--------|----------|----------|------------------------|
| Virtual Anger - Virtual Disgust    | L. Central/Temporal | S25 D6 hbt  | 3.565  | 1.033    | 3.452    | 0.019                  |
| Virtual Anger - Virtual Sadness    | L. Occipital        | S23 D15 hbt | -4.589 | 1.018    | -4.508   | 0.001                  |
| Virtual Disgust - Virtual Sadness  | L. Frontal          | S4 D6 hbt   | 4.125  | 1.044    | 3.950    | 0.008                  |
| Virtual Disgust - Virtual Surprise | L. Occipital        | S23 D15 hbt | 3.761  | 1.001    | 3.758    | 0.018                  |
| Virtual Sadness - Virtual Surprise | L. Occipital        | S23 D15 hbt | 3.768  | 0.978    | 3.853    | 0.012                  |

## Appendix B

# Functional Connectivity Contrasts

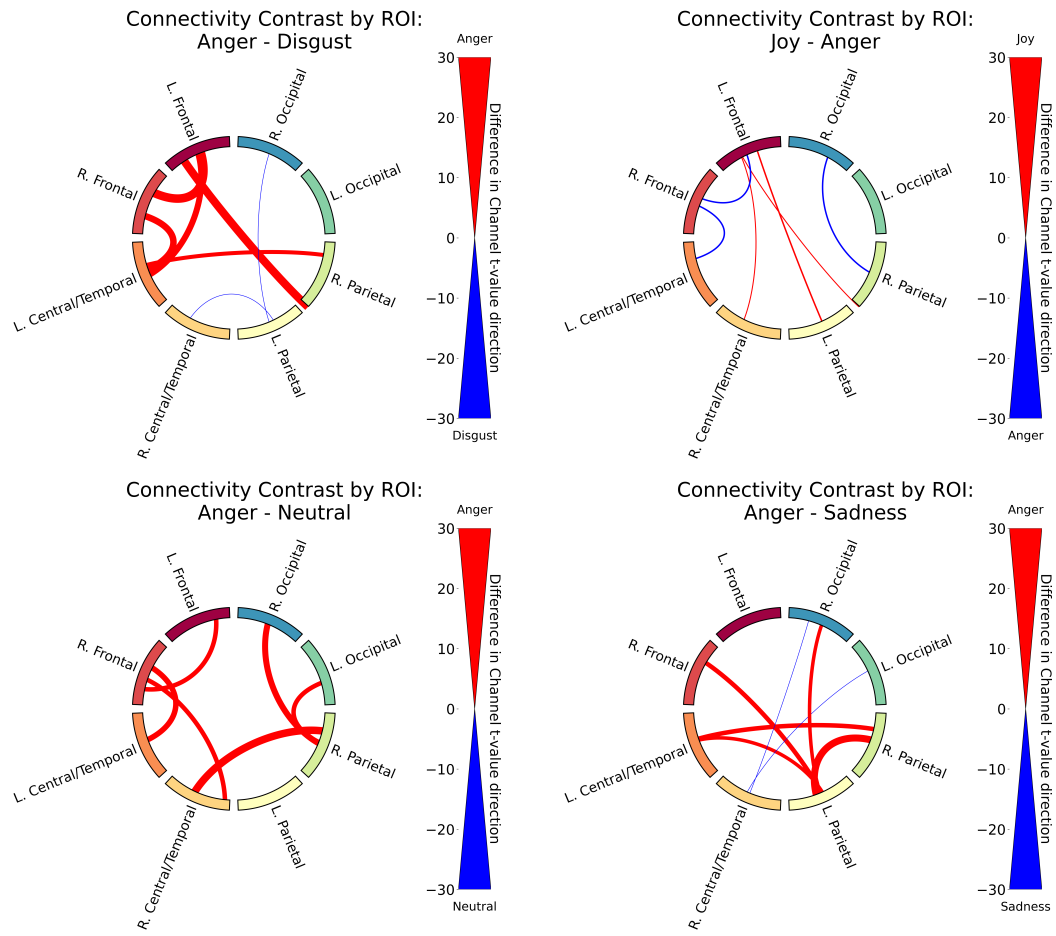
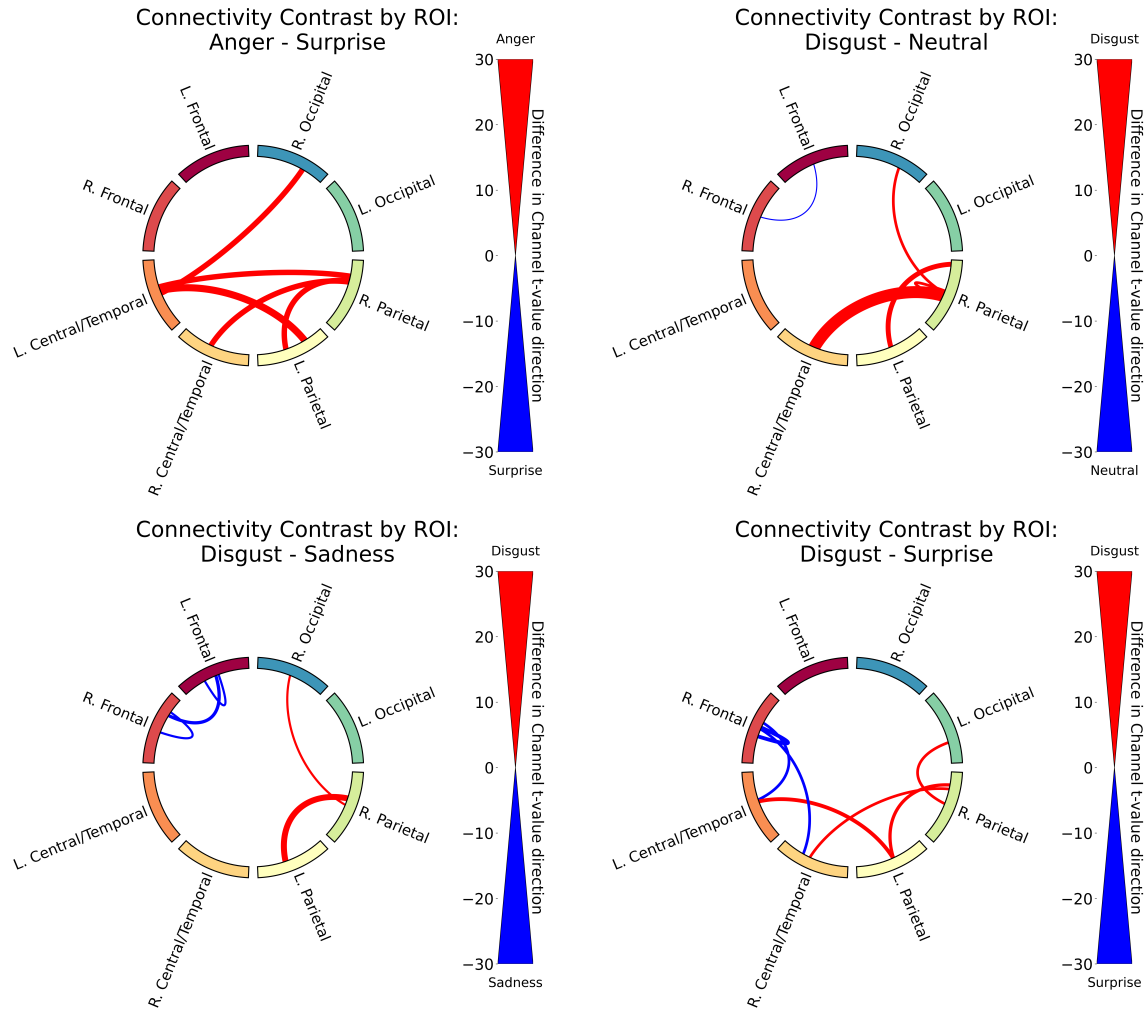
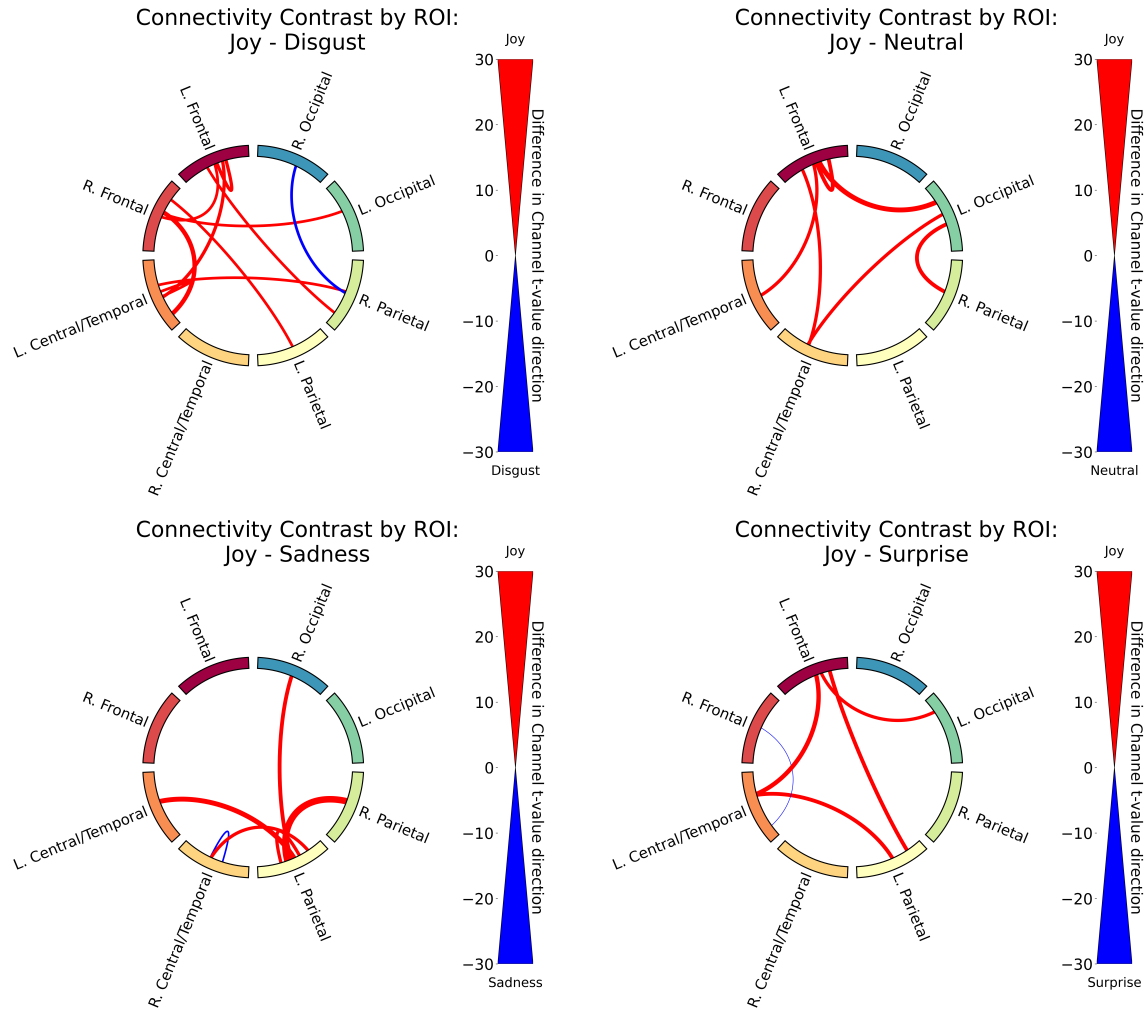


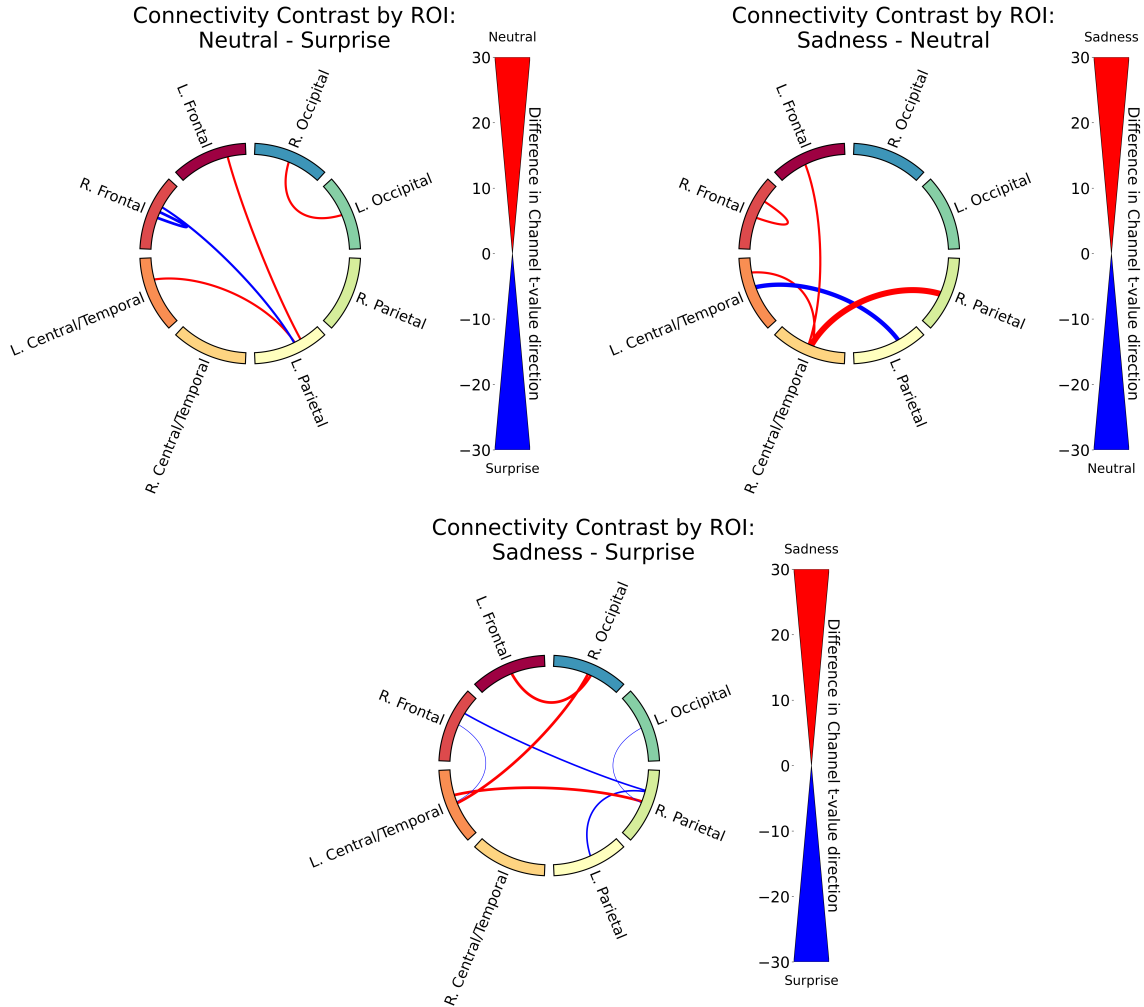
Figure B.1: Functional connectivity results for Anger contrasts: Anger vs. Disgust, Joy, Neutral, and Sadness. (1/4)



Functional connectivity results for Anger vs. Surprise and Disgust contrasts: Disgust vs. Neutral, Sadness, and Surprise. (2/4)



Functional connectivity results for Joy contrasts: Joy vs. Disgust, Neutral, Sadness, and Surprise. (3/4)



Functional connectivity results for Neutral and Sadness contrasts: Neutral vs. Surprise, Sadness vs. Neutral, and Sadness vs. Surprise. (4/4)

Table B.1: Ratio of positive to negative  $t$ -values for each contrast. The ratio is calculated as  $\text{Ratio} = (\text{Number of Positive } t\text{-values} - \text{Number of Negative } t\text{-values}) / (\text{Number of Positive } t\text{-values} + \text{Number of Negative } t\text{-values})$ . For condition1 - condition2, a positive ratio indicates that condition1 has more positive  $t$ -values than condition2, while a negative ratio indicates the opposite.

| Contrast       | Ratio  |
|----------------|--------|
| Real - Virtual | 0.632  |
| Joy - Fear     | -0.797 |

Continued on next page

Table B.1: Ratio of positive to negative  $t$ -values for each contrast. The ratio is calculated as  $\text{Ratio} = (\text{Number of Positive } t\text{-values} - \text{Number of Negative } t\text{-values}) / (\text{Number of Positive } t\text{-values} + \text{Number of Negative } t\text{-values})$ . For condition1 - condition2, a positive ratio indicates that condition1 has more positive  $t$ -values than condition2, while a negative ratio indicates the opposite.

| Contrast           | Ratio  |
|--------------------|--------|
| Joy - Anger        | -0.323 |
| Joy - Disgust      | 0.541  |
| Joy - Sadness      | 0.622  |
| Joy - Neutral      | 0.894  |
| Joy - Surprise     | 0.976  |
| Fear - Anger       | 0.345  |
| Fear - Disgust     | 0.959  |
| Fear - Sadness     | 0.865  |
| Fear - Neutral     | 0.977  |
| Fear - Surprise    | 0.966  |
| Anger - Disgust    | 0.805  |
| Anger - Sadness    | 0.709  |
| Anger - Neutral    | 0.957  |
| Anger - Surprise   | 0.897  |
| Disgust - Sadness  | 0.099  |
| Disgust - Neutral  | 0.677  |
| Disgust - Surprise | 0.172  |
| Sadness - Neutral  | 0.311  |
| Sadness - Surprise | 0.400  |
| Neutral - Surprise | 0.077  |

Continued on next page

Table B.1: Ratio of positive to negative  $t$ -values for each contrast. The ratio is calculated as  $\text{Ratio} = (\text{Number of Positive } t\text{-values} - \text{Number of Negative } t\text{-values}) / (\text{Number of Positive } t\text{-values} + \text{Number of Negative } t\text{-values})$ . For condition1 - condition2, a positive ratio indicates that condition1 has more positive  $t$ -values than condition2, while a negative ratio indicates the opposite.

| Contrast                    | Ratio  |
|-----------------------------|--------|
| Real Joy - Real Fear        | -0.284 |
| Real Joy - Real Anger       | -0.546 |
| Real Joy - Real Disgust     | 0.881  |
| Real Joy - Real Sadness     | -0.390 |
| Real Joy - Real Neutral     | 0.602  |
| Real Joy - Real Surprise    | 0.306  |
| Real Joy - Virtual Joy      | 0.400  |
| Real Joy - Virtual Fear     | -0.882 |
| Real Joy - Virtual Anger    | -0.985 |
| Real Joy - Virtual Disgust  | -0.636 |
| Real Joy - Virtual Sadness  | 0.161  |
| Real Joy - Virtual Neutral  | 0.158  |
| Real Joy - Virtual Surprise | 0.624  |
| Real Fear - Real Anger      | -0.254 |
| Real Fear - Real Disgust    | 0.832  |
| Real Fear - Real Sadness    | -0.016 |
| Real Fear - Real Neutral    | 0.617  |
| Real Fear - Real Surprise   | 0.400  |
| Real Fear - Virtual Joy     | 0.395  |
| Real Fear - Virtual Fear    | -0.578 |

Continued on next page

Table B.1: Ratio of positive to negative  $t$ -values for each contrast. The ratio is calculated as  $\text{Ratio} = (\text{Number of Positive } t\text{-values} - \text{Number of Negative } t\text{-values}) / (\text{Number of Positive } t\text{-values} + \text{Number of Negative } t\text{-values})$ . For condition1 - condition2, a positive ratio indicates that condition1 has more positive  $t$ -values than condition2, while a negative ratio indicates the opposite.

| Contrast                      | Ratio  |
|-------------------------------|--------|
| Real Fear - Virtual Anger     | -0.880 |
| Real Fear - Virtual Disgust   | 0.103  |
| Real Fear - Virtual Sadness   | 0.525  |
| Real Fear - Virtual Neutral   | 0.366  |
| Real Fear - Virtual Surprise  | 0.779  |
| Real Anger - Real Disgust     | 0.823  |
| Real Anger - Real Sadness     | 0.115  |
| Real Anger - Real Neutral     | 0.853  |
| Real Anger - Real Surprise    | 0.739  |
| Real Anger - Virtual Joy      | 0.858  |
| Real Anger - Virtual Fear     | -0.482 |
| Real Anger - Virtual Anger    | -0.914 |
| Real Anger - Virtual Disgust  | 0.359  |
| Real Anger - Virtual Sadness  | 0.507  |
| Real Anger - Virtual Neutral  | 0.743  |
| Real Anger - Virtual Surprise | 0.659  |
| Real Disgust - Real Sadness   | -0.792 |
| Real Disgust - Real Neutral   | 0.306  |
| Real Disgust - Real Surprise  | -0.400 |
| Real Disgust - Virtual Joy    | -0.188 |

Continued on next page

Table B.1: Ratio of positive to negative  $t$ -values for each contrast. The ratio is calculated as  $\text{Ratio} = (\text{Number of Positive } t\text{-values} - \text{Number of Negative } t\text{-values}) / (\text{Number of Positive } t\text{-values} + \text{Number of Negative } t\text{-values})$ . For condition1 - condition2, a positive ratio indicates that condition1 has more positive  $t$ -values than condition2, while a negative ratio indicates the opposite.

| Contrast                        | Ratio  |
|---------------------------------|--------|
| Real Disgust - Virtual Fear     | -0.959 |
| Real Disgust - Virtual Anger    | -0.979 |
| Real Disgust - Virtual Disgust  | -0.545 |
| Real Disgust - Virtual Sadness  | -0.372 |
| Real Disgust - Virtual Neutral  | -0.373 |
| Real Disgust - Virtual Surprise | -0.275 |
| Real Sadness - Real Neutral     | 0.859  |
| Real Sadness - Real Surprise    | 0.649  |
| Real Sadness - Virtual Joy      | 0.694  |
| Real Sadness - Virtual Fear     | -0.333 |
| Real Sadness - Virtual Anger    | -0.825 |
| Real Sadness - Virtual Disgust  | 0.036  |
| Real Sadness - Virtual Sadness  | 0.308  |
| Real Sadness - Virtual Neutral  | 0.489  |
| Real Sadness - Virtual Surprise | 0.885  |
| Real Neutral - Real Surprise    | -0.480 |
| Real Neutral - Virtual Joy      | -0.463 |
| Real Neutral - Virtual Fear     | -0.937 |
| Real Neutral - Virtual Anger    | -0.969 |
| Real Neutral - Virtual Disgust  | -0.856 |

Continued on next page

Table B.1: Ratio of positive to negative  $t$ -values for each contrast. The ratio is calculated as  $\text{Ratio} = (\text{Number of Positive } t\text{-values} - \text{Number of Negative } t\text{-values}) / (\text{Number of Positive } t\text{-values} + \text{Number of Negative } t\text{-values})$ . For condition1 - condition2, a positive ratio indicates that condition1 has more positive  $t$ -values than condition2, while a negative ratio indicates the opposite.

| Contrast                         | Ratio  |
|----------------------------------|--------|
| Real Neutral - Virtual Sadness   | -0.550 |
| Real Neutral - Virtual Neutral   | -0.588 |
| Real Neutral - Virtual Surprise  | -0.105 |
| Real Surprise - Virtual Joy      | 0.267  |
| Real Surprise - Virtual Fear     | -0.912 |
| Real Surprise - Virtual Anger    | -0.928 |
| Real Surprise - Virtual Disgust  | -0.200 |
| Real Surprise - Virtual Sadness  | 0.123  |
| Real Surprise - Virtual Neutral  | 0.058  |
| Real Surprise - Virtual Surprise | 0.432  |
| Virtual Joy - Virtual Fear       | -0.867 |
| Virtual Joy - Virtual Anger      | -0.979 |
| Virtual Joy - Virtual Disgust    | -0.767 |
| Virtual Joy - Virtual Sadness    | -0.203 |
| Virtual Joy - Virtual Neutral    | -0.476 |
| Virtual Joy - Virtual Surprise   | -0.150 |
| Virtual Fear - Virtual Anger     | -0.686 |
| Virtual Fear - Virtual Disgust   | 0.722  |
| Virtual Fear - Virtual Sadness   | 0.728  |
| Virtual Fear - Virtual Neutral   | 0.877  |

Continued on next page

Table B.1: Ratio of positive to negative  $t$ -values for each contrast. The ratio is calculated as  $\text{Ratio} = (\text{Number of Positive } t\text{-values} - \text{Number of Negative } t\text{-values}) / (\text{Number of Positive } t\text{-values} + \text{Number of Negative } t\text{-values})$ . For condition1 - condition2, a positive ratio indicates that condition1 has more positive  $t$ -values than condition2, while a negative ratio indicates the opposite.

| Contrast                           | Ratio  |
|------------------------------------|--------|
| Virtual Fear - Virtual Surprise    | 0.908  |
| Virtual Anger - Virtual Disgust    | 0.870  |
| Virtual Anger - Virtual Sadness    | 0.941  |
| Virtual Anger - Virtual Neutral    | 0.938  |
| Virtual Anger - Virtual Surprise   | 0.990  |
| Virtual Disgust - Virtual Sadness  | 0.351  |
| Virtual Disgust - Virtual Neutral  | 0.436  |
| Virtual Disgust - Virtual Surprise | 0.739  |
| Virtual Sadness - Virtual Neutral  | -0.020 |
| Virtual Sadness - Virtual Surprise | 0.561  |
| Virtual Neutral - Virtual Surprise | 0.515  |

# Appendix C

## Memory Task

### C.1 ANOVA Results

Table C.1: Two-way ANOVA results for the effect of Face Type and Emotion and their interaction on the correct responses.

|                         | sum_sq    | df         | F          | PR(>F)  |
|-------------------------|-----------|------------|------------|---------|
| Intercept               | 261.07756 | 1.00000    | 1764.58989 | 0.00000 |
| C(Face_Type)            | 1.17722   | 1.00000    | 7.95666    | 0.00481 |
| C(Emotion)              | 0.73335   | 6.00000    | 0.82610    | 0.54946 |
| C(Face_Type):C(Emotion) | 0.40872   | 6.00000    | 0.46041    | 0.83797 |
| Residual                | 710.47356 | 4802.00000 |            |         |

## C.2 Memory Task No Response Distribution

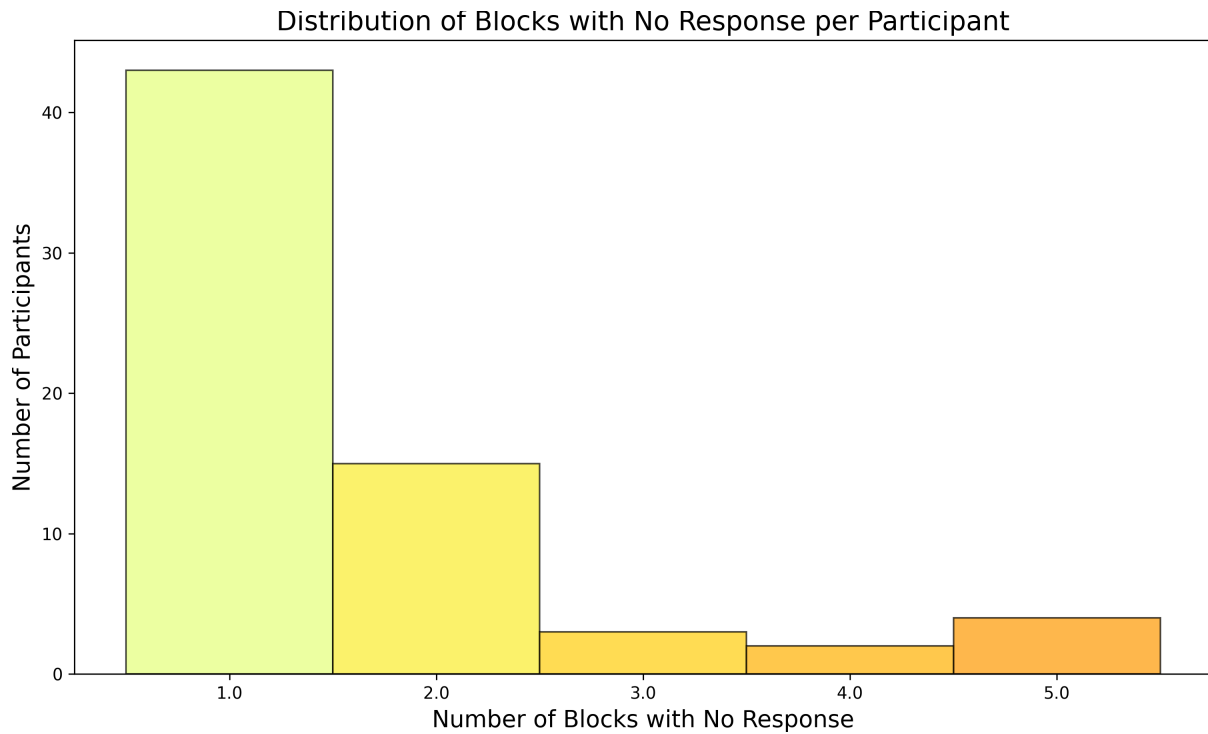


Figure C.1: Distribution of the number of no responses across the 56 blocks for each participant in the memory task.

## **Appendix D**

### **Ethics Approval Letters**

## D.1 REB Approval



### FW: Approval Notice - REB File #17656 (Conditions from 2024/02/01 have been addressed)

From Bobby Stojanowski <Bobby.Stojanowski@ontariotechu.ca>

Date Wed 8/14/2024 9:49 AM

To Dylan Rapanan <Dylan.Rapanan@ontariotechu.ca>; Steven Livingstone <Steven.Livingstone@ontariotechu.ca>

--

Bobby Stojanowski, Ph.D.  
Assistant Professor  
Faculty of Social Science and Humanities  
Ontario Tech University  
Oshawa, Ontario L1G 0C5

Adjunct Research Professor  
Department of Psychology and Brain and Mind Institute  
Western University  
London, ON, N6A 3K7

---

**From:** "researchethics@ontariotechu.ca" <researchethics@ontariotechu.ca>

**Date:** Tuesday, August 13, 2024 at 2:49 PM

**To:** Bobby Stojanowski <Bobby.Stojanowski@ontariotechu.ca>

**Cc:** "Whitaker Zedd(Student Lead/Post-Doctoral Lead)" <zedd.whitaker@ontariotechu.net>,  
"researchethics@ontariotechu.ca" <researchethics@ontariotechu.ca>

**Subject:** Approval Notice - REB File #17656 (Conditions from 2024/02/01 have been addressed)

Image removed by sender.

*Date:* August 13, 2024

*To:* Bobby Stojanowski

*From:* Joseph Eastwood, REB Chair

*File # & Title:* 17656 - Emotion Recognition in 2-D and 3-D images of human and virtual avatar faces

*Status:* APPROVED (Conditions from 2024/02/01 have been addressed)

*Review Type:* Delegated Review

*REB Expiry Date:* February 01, 2025

*Documents Approved:*

Figure D.1: First page of the REB Approval Letter.

| Document Type              | Document Name  | Version Date |
|----------------------------|--|--------------|
| Closure Letter             | Debriefing letter for participants that have completed the study.      | 2024/07/28   |
| Consent Letter             | Consent letter for participants  | 2024/07/28   |
| Data Collection Materials  | Appendix - Survey Questions & Task Sample - Amended (Clean)            |              |
| Response to Clarifications | Appendix including Questionnaire and sample trials from the experiment |              |

Notwithstanding this approval, you are required to obtain/submit, to Ontario Tech Research Ethics Board, any relevant approvals/permissions required, prior to commencement of this project.

The Ontario Tech Research Ethics Board (REB) has reviewed and approved the research study named above to ensure compliance with the Tri-Council Policy Statement: Ethical Conduct for Research Involving Humans (TCPS2), the Ontario Tech Research Ethics Policy and Procedures and associated regulations. As the Principal Investigator (PI), you are required to adhere to the research protocol described in the REB application as last reviewed and approved by the REB. In addition, **you are responsible for obtaining any further approvals that might be required to complete your project.**

Under the TCPS2, the PI is responsible for complying with the continuing research ethics reviews requirements listed below:

**Renewal Request Form:** All approved projects are subject to an annual renewal process. Projects must be renewed or closed by the expiry date indicated above ("Current Expiry"). Projects not renewed prior to the expiry date will be automatically suspended by the REB. If no response is received from suspended projects, the REB will permanently close your study for administrative non-compliance at the next scheduled REB meeting. Once your file has been formally closed, a new submission will be required to open a new file.

**Change Request Form:** If the research plan, methods, and/or recruitment methods should change, please submit a change request application to the REB for review and approval prior to implementing the changes.

**Adverse or Unexpected Events Form:** Events must be reported to the REB within 72 hours after the event occurred with an indication of how these events affect (in the view of the Principal Investigator) the safety of the participants and the continuation of the protocol (i.e. un-anticipated or un-mitigated physical, social or psychological harm to a participant).

**Research Project Completion Form:** This form must be completed when the research study is concluded.

Always quote your REB file number (**17656**) on future correspondence. We wish you success with your study.

Sincerely,

Joseph Eastwood, PhD  
REB Chair  
[Joseph.Eastwood@ontariotechu.ca](mailto:Joseph.Eastwood@ontariotechu.ca)

Figure D.2: Second page of the REB Approval Letter.

## D.2 REB Renewal



---

**FW: REB Renewal Approved - 17656**

---

**From:** Bobby Stojanoski <Bobby.Stojanoski@ontariotechu.ca>

**Date:** Mon 1/13/2025 10:15 PM

**To:** Dylan Rapanan <Dylan.Rapanan@ontariotechu.ca>

--  
Bobby Stojanoski, Ph.D.  
Research Excellence Chair in Developmental Neuroscience  
Assistant Professor  
Faculty of Social Science and Humanities  
Ontario Tech University  
Oshawa, Ontario L1G 0C5

Adjunct Research Professor  
Department of Psychology and Brain and Mind Institute  
Western University  
London, ON, N6A 3K7

---

**From:** "researchethics@ontariotechu.ca" <researchethics@ontariotechu.ca>

**Date:** Monday, November 18, 2024 at 1:00 PM

**To:** Bobby Stojanoski <Bobby.Stojanoski@ontariotechu.ca>

**Cc:** "Whitaker Zedd(Student Lead/Post-Doctoral Lead)" <zedd.whitaker@ontariotechu.net>, "researchethics@ontariotechu.ca" <researchethics@ontariotechu.ca>

**Subject:** REB Renewal Approved - 17656

[REDACTED]

**Date:** November 18, 2024

**To:** Bobby Stojanoski

**From:** Research Ethics Office

**REB File #:** 17656

**Project Title:** Emotion Recognition in 2-D and 3-D images of human and virtual avatar faces

**Current Expiry:** November 01, 2025

---

The research ethics file named above has been renewed. You are required to continue to adhere to the protocol as last reviewed and approved by Ontario Tech's Research Ethics Board (REB). This research is subject to review

Figure D.3: First page of the REB Renewal Request Approval Letter.

requirements. This research file must be renewed or closed by the current expiry date (**November 01, 2025**) by using the following forms from the [IRIS research portal](#).

- **Renewal Request Form:** All approved projects are subject to an annual renewal process. Projects must be renewed or closed by the expiry date indicated above (“Current Expiry”). Projects not renewed prior to the expiry date will be automatically suspended by the REB. If no response is received from suspended projects, the REB will permanently close your study for administrative non-compliance at the next scheduled REB meeting. Once your file has been formally closed, a new submission will be required to open a new file.
- **Change Request Form:** All changes or modifications (e.g., adding a team member or a change in methodology) to your study must be submitted via a change request form and approved by the REB.
- **Adverse or Unexpected Events Form:** Events must be reported to the REB within 72 hours with an indication of how these events affect, in the view of the principal investigator, the safety of the participants and the continuation of the protocol (e.g., unanticipated or unmitigated physical, social or psychological harm to a participant).
- **Research Project Completion Form:** This form must be completed when the research study concludes.

**Always quote your REB file number (17656) on future correspondence.** If you are a student researcher, your supervisor has been copied to this message.

We wish you continued success with your study.

Figure D.4: Second page of the REB Renewal Request Approval Letter.